

GLOBULAR CLUSTER ABUNDANCES FROM HIGH-RESOLUTION, INTEGRATED-LIGHT SPECTROSCOPY. IV. THE LARGE MAGELLANIC CLOUD: α , FE-PEAK, LIGHT, AND HEAVY ELEMENTS¹

JANET E. COLUCCI

Department of Astronomy and Astrophysics, 1156 High Street, UCO/Lick Observatory,
University of California, Santa Cruz, CA 95064; jcolucci@ucolick.org

REBECCA A. BERNSTEIN

Department of Astronomy and Astrophysics, 1156 High Street, UCO/Lick Observatory,
University of California, Santa Cruz, CA 95064; rab@ucolick.org

SCOTT A. CAMERON

Science Department, 3000 College Heights Blvd., Cerro Coso Community College, Ridgecrest, CA 93555; scameron@cerrocoso.edu

AND

ANDREW MCWILLIAM

The Observatories of the Carnegie Institute of Washington, 813 Santa Barbara Street, Pasadena, CA 91101-1292; andy@ociw.edu

Accepted November 21, 2011 to Astrophysical Journal

ABSTRACT

We present detailed chemical abundances in 8 clusters in the Large Magellanic Cloud (LMC). We measure abundances of 22 elements for clusters spanning a range in age of 0.05 to 12 Gyr, providing a comprehensive picture of the chemical enrichment and star formation history of the LMC. The abundances were obtained from individual absorption lines using a new method for analysis of high resolution ($R \sim 25,000$) integrated light spectra of star clusters. This method was developed and presented in Papers I, II, and III of this series. In this paper, we develop an additional integrated light χ^2 -minimization spectral synthesis technique to facilitate measurement of weak (~ 15 mÅ) spectral lines and abundances in low signal-to-noise ratio data ($S/N \sim 30$). Additionally, we supplement the integrated light abundance measurements with detailed abundances that we measure for individual stars in the youngest clusters (Age < 2 Gyr) in our sample. In both the integrated light and stellar abundances we find evolution of $[\alpha/\text{Fe}]$ with $[\text{Fe}/\text{H}]$ and age. Fe-peak abundance ratios are similar to those in the Milky Way, with the exception of $[\text{Cu}/\text{Fe}]$ and $[\text{Mn}/\text{Fe}]$, which are sub-solar at high metallicities. The heavy elements Ba, La, Nd, Sm, and Eu are significantly enhanced in the youngest clusters. Also, the heavy to light s -process ratio is elevated relative to the Milky Way ($[\text{Ba}/\text{Y}] > +0.5$) and increases with decreasing age, indicating a strong contribution of low-metallicity AGB star ejecta to the inter-stellar medium throughout the later history of the LMC. We also find a correlation of integrated light Na and Al abundances with cluster mass, in the sense that more massive, older clusters, are enriched in the light elements Na and Al with respect to Fe, which implies that these clusters harbor star-to-star abundance variations as is common in the Milky Way. Lower mass, intermediate age and young clusters have Na and Al abundances that are lower and more consistent with LMC field stars. Our results can be used to constrain both future chemical evolution models for the LMC and theories of GC formation.

Subject headings: galaxies: individual (LMC) — galaxies: star clusters: general — galaxies: abundances — globular clusters: individual (NGC 2005, NGC 2019, NGC 1916, NGC 1978, NGC 1718, NGC 1866, NGC 1711, NGC 2100) — stars: abundances

1. INTRODUCTION

We are conducting an ongoing program to obtain detailed abundances from high resolution ($R \sim 25,000$), integrated light (IL) spectra of extragalactic star clusters. In a series of papers, we have developed and presented a method to obtain abundances of ~ 20 elements from individual absorption lines in these spectra. In McWilliam & Bernstein (2008) and Cameron (2009), hereafter Paper I and Paper II, we developed this method on a training set of 7 globular clusters (GCs) in the Milky

Way (MW), which have ages > 10 Gyr. In Colucci et al. (2011) and Colucci & Bernstein (2011, submitted), hereafter Paper III and CB11, we extended this method to a training set of 8 massive, high surface brightness star clusters in the Large Magellanic Cloud (LMC), for which we obtained measurements of $[\text{Fe}/\text{H}]$ and age. This sample of LMC clusters is critical for development of the IL spectra method on clusters with ages between 0.05 and 10 Gyrs, because the MW has few, if any, massive high surface brightness clusters in this age regime. In this paper, we present detailed chemical abundances of ~ 20 additional elements in the LMC training set clusters.

The IL method was designed to take advantage of

¹ This paper includes data gathered with the 6.5 meter Magellan Telescopes located at Las Campanas Observatory, Chile.

the high luminosities and surface brightness of unresolved GCs, as compared to individual stars, in order to study chemical evolution and cluster properties in distant galaxies (~ 4 Mpc). Therefore, the purpose of developing this technique is to use GCs to constrain galaxy evolution in the same way that stars have been used to constrain formation of the MW. It has been demonstrated that star clusters trace the properties of major star formation events in their host galaxies, and therefore they are crucial tools for learning about more distant galaxies where individual stars cannot be studied in detail (e.g. Brodie & Strader 2006).

To this end, it is important to verify that our IL spectral analysis provides accurate results for clusters of all ages. The study of young clusters, like those in our LMC training set, is particularly interesting for several reasons. First, there are young massive star clusters currently forming in nearby star-bursting galaxies like M82, which can teach us about cluster formation in conditions of high star formation rate and intensity. These conditions are likely similar to those present at high redshift, and are important for understanding the formation of massive clusters in general (e.g. Leitherer 2001). Young clusters are also interesting in light of the recent results that MW GCs have small age and abundance spreads, and thus had multiple, fast star formation episodes at early times (e.g. Piotto et al. 2007; Mackey et al. 2008; Milone et al. 2009; Goudfrooij et al. 2011; D’Ercole et al. 2008; Carretta et al. 2010; Decressin et al. 2007; de Mink et al. 2009; Conroy & Spergel 2011; Conroy 2011). By studying IL abundance trends with age and mass in these young clusters we can try and constrain cluster formation timescales and internal chemical enrichment models. Additionally, in starbursting environments young clusters allow us to study the intrinsic cluster luminosity function and cluster disruption, which can be used to constrain the contribution of cluster stars to field star populations.

Our training set of clusters in the LMC not only provides a necessary test of the IL method on young clusters, but also comprehensive information on the chemical evolution of the LMC itself over a wide range in age and $[\text{Fe}/\text{H}]$. While the star formation history (SFH) of the LMC field and cluster populations has been well-studied photometrically and with low resolution spectra (e.g. Harris & Zaritsky 2009; Olszewski et al. 1996; Cioni et al. 2006; Carrera et al. 2008; Olszewski et al. 1991), detailed abundance information for the LMC is much more limited than for the MW. This is simply due to the long integration times required to obtain high S/N, high resolution spectra of large samples of stars at the distance of the LMC ($D \sim 50$ kpc).

From prior work with high resolution photometry, we know that the LMC cluster system had its initial formation epic >10 Gyr ago, and at least one additional burst 2-4 Gyr ago (e.g. Bica et al. 1986; Olszewski et al. 1991; Harris & Zaritsky 2009). There is only one cluster that formed in the “age-gap” between 3-10 Gyr. The disk field population seems to have had a nearly constant formation rate over most of the history of the LMC, with evidence of localized enhancement in star formation rate 1-4 Gyrs ago (e.g. Geha et al. 1998). The LMC also has a high surface brightness bar, which shows an underly-

ing old population, and some evidence for a burst in star formation ~ 6 Gyr ago (Cole et al. 2000).

With detailed chemical abundances, we can further constrain the SFH of the LMC. There are several useful galaxy formation diagnostics that can be used when large samples of elements are available. One common focus of detailed abundance studies is to obtain α -element abundances (e.g. O, Mg, Ca, Si, Ti), which are produced mostly in Type II supernovae (SNe II), or massive stars, on short timescales. Large over-abundances (with respect to Fe-peak elements) of α -elements are therefore signatures of early, rapid or bursty star formation (e.g. Tinsley 1979; Woosley & Weaver 1995). Another useful diagnostic is the ratio of $[\text{Ba}/\text{Y}]$. The high $[\text{Ba}/\text{Y}]$ ratios observed in nearby dwarf galaxies (e.g. Shetrone et al. 2001, 2003; Smecker-Hane & McWilliam 2002; McWilliam & Smecker-Hane 2005; Geisler et al. 2007; Tolstoy et al. 2009) reflect the metallicity dependence of the s -process in asymptotic giant branch (AGB) stars (e.g. Busso et al. 1999). This metallicity dependence means that high $[\text{Ba}/\text{Y}]$ ratios identify star formation that occurred in long-lived low-metallicity environments, or low star formation rates. High $[\text{Ba}/\text{Y}]$ ratios have previously been observed in individual stars in the LMC (Pompéia et al. 2008; Mucciarelli et al. 2008), and we determine new $[\text{Ba}/\text{Y}]$ ratios for the 8 clusters analyzed in this work.

In this paper, our goals are both to demonstrate the accuracy of our abundance analysis when applied to young clusters, and also to obtain new abundance results for LMC clusters in order to study the chemical evolution history of the LMC. In §2 we present the observations and data reduction. In §3 we review the IL abundance analysis, results from Paper III, and present a new, supplementary IL spectral synthesis technique. In §4, we present abundance results from the sample of individual stars in CB11, which are used to verify the precision of the IL method at young ages. IL chemical abundance results are presented in §5. In §6 we discuss our results compared to abundance analyses from the literature. In §7, §8 and §9 we discuss the implications of our results for massive cluster formation and the formation and evolution of the LMC. Throughout this work we will frequently refer to previous measurements of abundances in individual LMC stars by Pompéia et al. (2008), Johnson et al. (2006), Mucciarelli et al. (2008), Mucciarelli et al. (2010), Mucciarelli et al. (2011), Luck & Lambert (1992), Russell & Bessell (1989), Hill et al. (2000) and Hill et al. (1995), which will be abbreviated as P08, J06, M08, M10, M11, LL92, RB89, H00, and H95, respectively.

2. OBSERVATIONS AND DATA REDUCTION

Integrated light spectra for all of the LMC clusters were obtained by uniformly scanning the core regions of each cluster. All spectra were obtained with the 2.5 m du Pont telescope at Las Campanas in 2000 December and 2001 January, as described in Paper I, Paper II and Paper III, with the exception of NGC 1718 which was observed with the MIKE double echelle spectrograph (Bernstein et al. 2003) on the 6.5 m Magellan telescope in 2006 November. The reduction of data from the du Pont telescope is described fully in Paper I. The reduction of the data from the Magellan telescope is described fully in Paper III.

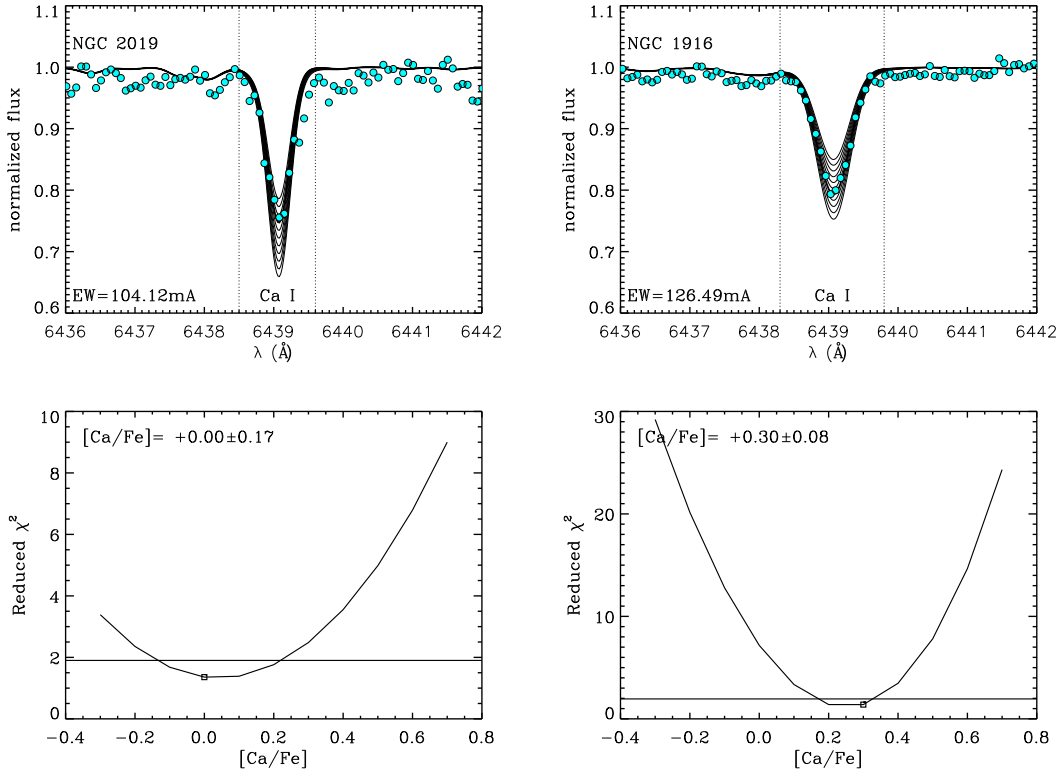


Figure 1. Example of χ^2 minimization technique for the Ca I 6439 Å line for NGC 2019 (left panels) and NGC 1916 (right panels). The top panels show the observed data as cyan filled circles, and solid black lines show the IL synthesized spectra corresponding to $-0.3 < [Ca/Fe] < +0.7$. The thick black line in each figure shows the IL spectrum corresponding to the minimum in the reduced χ^2 , which can be seen in the bottom panels as a function of $[Ca/Fe]$.

The LMC training set includes 8 clusters that are well enough sampled to have well-constrained $[Fe/H]$ and ages from our analysis in Paper III (NGC 1916, NGC 2005, NGC 1916, NGC 1718, NGC 1978, NGC 1866, NGC 1711, and NGC 2100). These clusters were chosen to span the available range in age and $[Fe/H]$ of high surface brightness clusters found in the LMC. In Paper III we divided the LMC clusters into three groups according to age. “Old” clusters are those with ages >5 Gyr, “intermediate age” clusters are those with ages 1–4 Gyr, and “young” clusters are those with ages <1 Gyr. The clusters in each group are listed in Table 1.

In CB11 we presented an analysis of the $[Fe/H]$ of 10 cool giant stars in the intermediate and young clusters of our sample. The stellar sample includes 2 stars in NGC 1978, 3 stars in NGC 1866, 3 stars in NGC 1711, and 2 stars in NGC 2100. All of the stellar spectra were taken with the MIKE spectrograph on Magellan. The description of the target selection, data reduction, and stellar parameter analysis is presented in CB11.

3. INTEGRATED LIGHT ABUNDANCE ANALYSIS

The IL abundance analysis technique is described in detail in Paper I, II and III and CB11, and will not be repeated here. In § 3.1, we briefly summarize the ages and $[Fe/H]$ derived for the LMC training set clusters in Paper III and CB11. In § 3.2–§ 3.3, we present the line lists we employ and discuss a new extension of the ILABUNDS code for determining abundances of individual lines with a χ^2 -minimization spectral synthesis technique.

3.1. CMDs and Ages

In Paper III and CB11 we presented a detailed analysis of the $[Fe/H]$ and age solutions for each cluster in the LMC training set. The $[Fe/H]$ and age for each cluster are used to create final, representative color magnitude diagrams (CMDs) from which we get the stellar parameters needed for spectral synthesis and abundance determination (see Papers I, II and III). Here we use these final representative CMDs with the age and $[Fe/H]$ derived in Paper III and CB11 for each cluster to calculate abundances for the additional elements.

For the final $[Fe/H]$ and ages we use the results from Paper III for the old clusters, and the results from CB11 for the intermediate age and young clusters. These results are summarized in columns 3 and 4 in Table 1. We constrained the age of old clusters to a range of ~ 5 Gyrs, intermediate age clusters to ~ 1 -2 Gyr, and young clusters to ~ 0.4 Gyr. The acceptable age range for each cluster leads to a range in derived $[Fe/H]$, corresponding to the different stellar populations at each age. For old clusters, the difference in $[Fe/H]$ is generally small (<0.05 dex) because there are only subtle changes in the stellar populations at older ages. Therefore, for the old clusters we use one best-fitting CMD to report abundances calculated for other elements. For intermediate age and young clusters, which have more rapidly evolving stellar populations, the difference in derived abundances between CMDs of different ages can occasionally be larger than the line-to-line statistical scatter (σ_{lines}) of the individual Fe lines (>0.1 dex). For intermediate age and young

clusters, we adopt the mean abundances calculated from two CMDs spanning the appropriate age range and report an additional uncertainty on the abundances due to the assumed age as σ_{age} .

3.2. EWs and Line Lists

We use the semi-automated program GETJOB (McWilliam et al. 1995b) to measure absorption line equivalent widths (EWs) for individual lines in both the IL and stellar spectra. We interactively fit low order polynomials to continuum regions for each spectral order. The line profiles are fit with single, double, or triple Gaussians as needed.

Line lists and $\log gf$ values were taken from Paper I, Paper II, Colucci et al. (2009), and Meléndez & Barbuy (2009), and supplemented with the Kurucz atomic and molecular line database (Kurucz 1997). The same line list was used for analysis of both the cluster IL spectra and the individual stellar spectra. The lines and EWs measured in the cluster IL spectra are listed in Table 2, and the EWs measured in the stellar spectra are listed in Table 3.

In addition to the IL EW analysis used in our previous work, we have implemented an IL line synthesis component to ILABUNDS, which we describe in detail in § 3.3. Lines with abundances determined using the synthesis routine of ILABUNDS are labeled “SYN” in column 13 of Table 2, while abundances determined using our original EW analysis are labeled “EW.” We have calculated abundances with hyperfine splitting (hfs) of energy levels taken into account for the elements Sc, V, Co, Cu, Mn, Ba, Sr, La and Eu. These calculations are noted as “HFS” in Table 2 and Table 3.

3.3. ILABUNDS Line Synthesis

The development of the line synthesis routine for ILABUNDS was motivated by the desire to make additional measurements of poorly constrained elements by analyzing weak features for which EWs are not otherwise recoverable. As for the analysis of all of the elements discussed in this paper, the line synthesis routine is performed only with the best-fitting CMD already identified from the [Fe/H] analysis, as discussed above. We note that the goal of our synthesis analysis is still to calculate abundances for a given species using individual lines, not to fit the entire spectrum at one time. Therefore, we limit the synthesis region to $\pm 10 \text{ \AA}$ from the line of interest, and supplement our standard line lists with the Kurucz database.

Like the EW calculation routine of ILABUNDS, the synthesis component calculates spectra for each stellar type in the CMDs using the 2010 version of MOOG (Snedden 1973). The spectra for the representative stars are then flux weighted according to the scheme described for the EWs in Paper I. The combined synthesized IL spectrum is then renormalized and convolved with the 1-dimensional velocity dispersion (σ_v) of the cluster. The measurement of σ_v for the LMC clusters follows the method described in Colucci et al. (2009), and is presented in Colucci et al. (2012, in preparation).

A χ^2 -minimization scheme is used to determine the best-fitting abundance for a given line. First, the continuum level is identified in a 30-40 \AA window as the

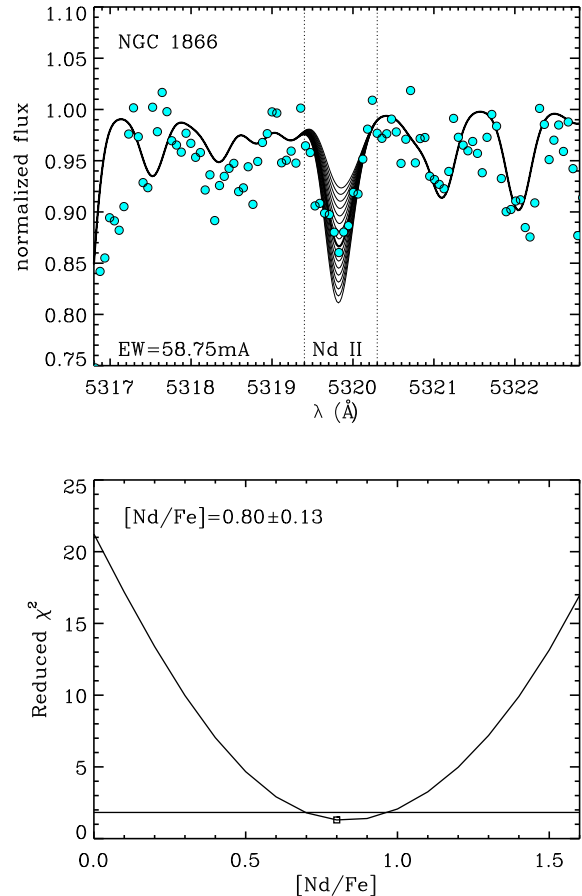


Figure 2. Example of the χ^2 -minimization technique for the Nd II 5319 \AA line for NGC 1866. In the top panel, the observed data is shown as filled circles, and the solid black lines show the IL synthesized spectra corresponding to $+0.0 < [\text{Nd}/\text{Fe}] < +1.6$. Bottom panel is the same as in Figure 1, only for Nd. This example shows a region with lower S/N and weaker features than that of Figure 1, and that the abundance is well determined with this technique.

mean value with 3σ lower rejection. Next, a 1 \AA region used for the χ^2 fitting must be identified by eye and adjusted on a cluster by cluster basis because of blending effects that vary due to the different σ_v and metallicities of the clusters. An example of how this region can vary between clusters because of different σ_v is shown in the top panels of Figure 1. The left panel shows the Ca I 6439 \AA line for NGC 2019 and the right panel shows the same for NGC 1916. The larger σ_v of NGC 1916 makes a larger region necessary for calculating the χ^2 . Note, the Ca I 6439 \AA line is a strong, high S/N line for which EWs can be accurately measured using GETJOB, and is shown here only as a demonstration of the χ^2 technique.

For a given line, synthesized spectra are created for a range of abundances and the reduced χ^2 is calculated for each. The minimum in the χ^2 can then be identified, as shown in the bottom panels of Figure 1. We determine the approximate uncertainty in abundance using the range of values that are within $\sim 40\%$ of the minimum χ^2 , shown by the horizontal solid lines in the bottom panels of Figure 1. EWs for synthesized lines are calculated for the best fitting spectra and are listed in Table 2. We find excellent agreement between the EWs

measured using GETJOB and the EWs measured with the χ^2 -minimization for the examples in Figure 1. For both NGC 2019 and NGC 1916 the EWs measured using the two techniques agree to within 1%.

As an example of a case in which the line synthesis is particularly useful, we show the χ^2 -minimization for a weak (15% flux decrement) Nd II line at 5319 Å in Figure 2. The Nd II line falls into the category of being in a low S/N region of the spectra. The line synthesis is useful anywhere line depths are reduced. This can occur in low S/N data, for clusters with high σ_v , and for weak transitions. While the uncertainty on the derived abundance of these synthesized lines is higher even when using the χ^2 -minimization technique, we are able to meaningfully constrain abundances of lines with EWs as small as 20 mÅ, or in data with S/N \sim 30. This additional technique makes it possible for us to use the IL abundance analysis method on lower S/N data of distant, unresolved clusters in future work.

4. ACCURACY OF LMC IL ANALYSIS: COMPARISON TO OUR SAMPLE OF INDIVIDUAL STARS IN YOUNG CLUSTERS

To demonstrate that the IL method produces accurate abundances for clusters with ages of 0.05 to 2 Gyr, we first compare the abundances measured with our IL abundance analysis method to the abundances measured in individual stars. These comparisons for NGC 1978, NGC 1866, NGC 1711, and NGC 2100 are shown in Figure 3. Wherever possible we have used the same analysis techniques, i.e. identical line lists, line parameters, stellar atmospheres, and stellar spectral synthesis codes. This eliminates many potential systematic offsets that can be present when comparing our cluster IL results to abundance analyses performed by other authors (see § 6 for more details).

In Figure 3 we show the comparison between the results obtained from individual stars in NGC 1978, NGC 1866, NGC 1711, and NGC 2100 to the results obtained from the IL spectra in those same clusters. To evaluate systematic offsets between the two methods, we have performed linear least squares fits, with the slopes constrained to unity, to both the neutral and ionized species in each cluster. To show the scatter around the fits we also show the residuals in the bottom panels of the plots. The derived offset and scatter for the neutral and ionized lines for each cluster are listed in Table 4. We find that the systematic offset in neutral species is <0.1 dex in all cases except for NGC 1711, for which we only have three elements available for comparison. The scatter about the fits for neutral species is 0.40, 0.17, 0.18, and 0.29 dex for NGC 1978, 1866, 1711, and 2100, respectively. For ionized species the average systematic offset is <0.16 dex in all cases, and the scatter is 0.33, 0.22, and 0.26 dex for NGC 1978, 1866, and 2100, respectively. In both the neutral and ionized cases the scatter about the fits is comparable to the σ_{Tot} of the cluster measurements, and it is likely that with higher S/N IL spectra the scatter would decrease. For example, the cluster for which we have the highest S/N data in the IL spectra, NGC 1866, has the smallest scatter in both neutral and ionized species.

For each cluster in Figure 3 we can look for element species that are outliers in the fits. It is interesting to

note if the outliers for all of the clusters tend to be of the same species, which would mean that the IL analysis method has a large systematic error for these particular species. For NGC 1978 the outliers are Na I, Ti I, Mn I and Nd II. For NGC 1866 the only outlier is Sm II. For NGC 1711 we only have four elements available for comparison, with no obvious outliers. For NGC 2100 the outliers are Al I and Ba II. This comparison shows that the outliers in each cluster are different, so it does not appear that the IL method has a large systematic offset for any particular element, with the caveat that we can only make this detailed comparison for the clusters in our sample that have ages < 2 Gyr, due to the ages of our current sample of individual stars.

Finally, it is particularly interesting to look at the comparison for the youngest cluster in our sample, NGC 2100. For this cluster we were only able to measure an upper limit in [Fe/H] (Paper III; CB11), which we found to be ~ 0.4 dex more metal-rich than the mean [Fe/H] we found from the two stars c12 and b22. From inspection of Figure 3, we find that even though the [Fe/H] is offset by $+0.4$ dex, the abundance ratios are extremely consistent with the abundance ratios that we derive for the individual stars. This is not unexpected, because the relative abundances of elements with respect to Fe change very slowly, even when the absolute changes are more significant. This is also consistent with what we found in Colucci et al. (2009) for old clusters in M31. Therefore, the IL analysis method can provide reliable measurements of the abundance ratios even when we can only obtain a limit on the [Fe/H].

In conclusion, we find good agreement between the abundance ratios measured from the cluster IL spectra and the abundance ratios measured from the individual stellar spectra. The largest discrepancies are found for the cluster IL spectra with the lowest S/N. In this sample, there are no elements with abundances that are always predictably inconsistent between the IL and stellar analyses. We conclude that in general the cluster IL analysis method results in abundances that are accurate to $\lesssim 0.1$ dex over the age range 0.05–2 Gyr. The accuracy of the measured abundance for any species for any one cluster naturally depends on the accuracy of the measured equivalent widths, which in turn depend on the S/N of the data, the velocity dispersion of the cluster, and the strength of the constraint on the CMD solution. For the results in this paper, the abundances measured for any one species in any one cluster have statistical uncertainties of 0.05 – 0.3 dex (see columns for σ_{lines} , σ_{age} , and σ_{Tot} in Tables 5 through 12).

5. RESULTS & DISCUSSION : CHEMICAL ABUNDANCES

In the following sections we present abundance results in our LMC clusters for ~ 20 individual elements, including α -elements, light elements, Fe-peak elements, and neutron capture elements. We discuss the behavior of similar groups of elements with respect to previous abundance work in LMC clusters and field stars, as well as in comparison to abundance work in MW clusters and field stars. Many of the LMC abundances measured here are the first such measurements for certain clusters, and will be discussed further in §7, §8 and §10.

For the eight LMC clusters, we show the final IL abundances, number of available spectral lines and the uncer-

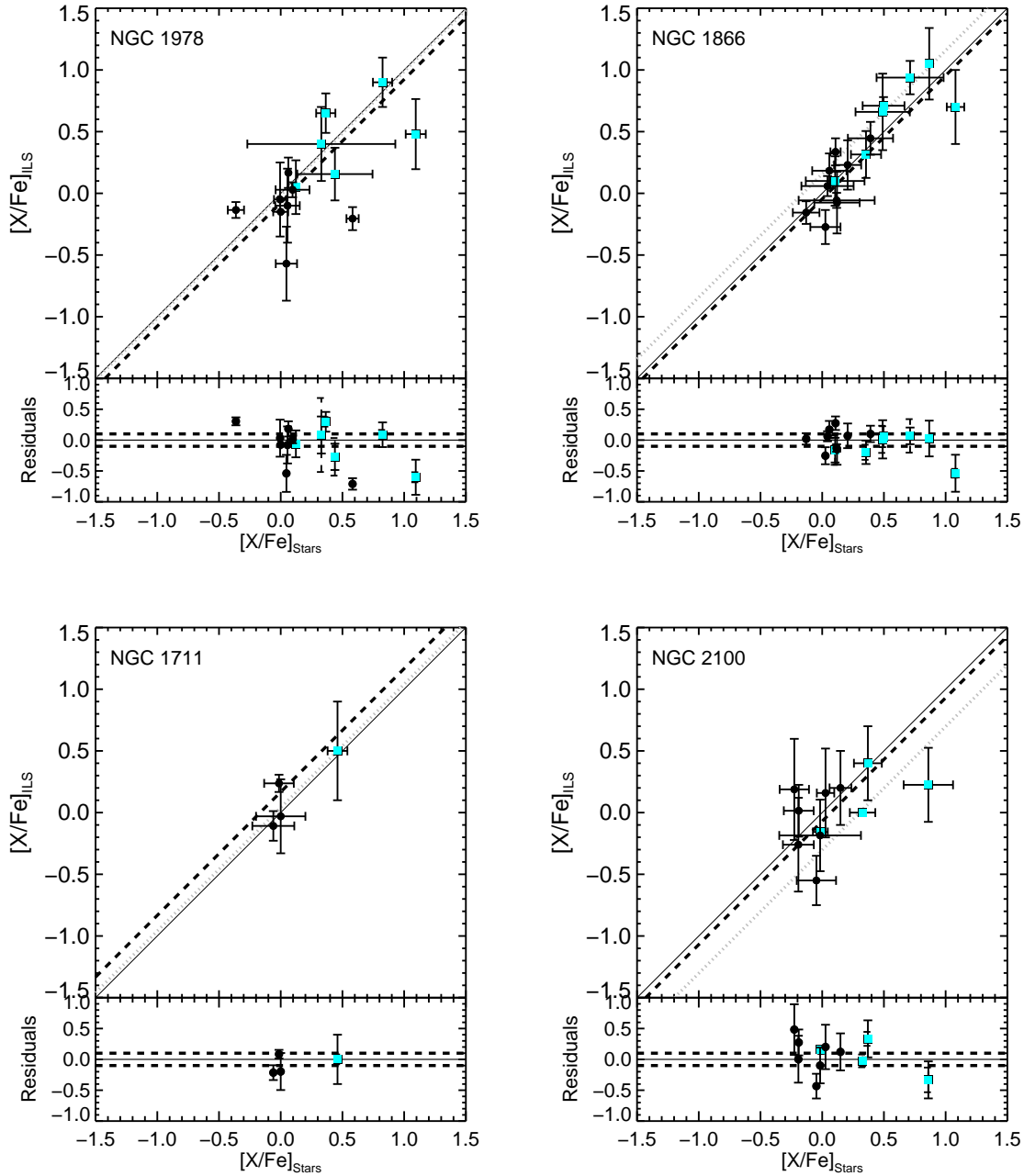


Figure 3. Comparison of abundance ratios from IL and stellar analysis for NGC 1978, NGC 1866, NGC 1711, and NGC 2100. Black circles and cyan squares show abundances for neutral and ionized species, respectively. The thick dashed line in the top panels of each plot shows a linear least squares fit to the neutral species, with the slope of the fit constrained to unity. The thin dotted line shows the same fit to the ionized species. The bottom panels in each plot show the residuals of the neutral and ionized species around their respective trend lines. The thick dashed lines in the bottom plots mark residuals of ± 0.1 dex, to guide the eye. In general the two methods agree to the ± 0.1 dex level.

tainty in the mean of N_{lines} ($\sigma_{lines} = \sigma / \sqrt{(N_{lines} - 1)}$) for each species in Tables 5 through 12. For the young and intermediate age clusters we also report the uncertainty in the $[X/Fe]$ ratios that results from the uncertainty in the age solution (σ_{age}). For the old clusters the uncertainty associated with the age of the cluster is small—usually $<< 0.05$ dex for $[X/Fe]$ —and so is not included for the individual species. Note that for the young and intermediate age clusters, age uncertainties are the dominant systematic uncertainty in the abundances, and the only systematic uncertainty that does not have an analogy in any calculation of abundances for individual stars. As in any stellar abundance analysis, systematic uncertainties due to the details of the calculations (e.g., assumptions adopted in MOOG, the Kurucz model atmospheres, α -enhancement effects on H γ opacity, gf -values) are unavoidable, difficult to quantify, and best dealt with by making uniform comparison between results (see §6). See previous papers in this series for further discussion.

The results for the 10 stars in the LMC clusters NGC 1978, NGC 1866, NGC 1711 and NGC 2100 are reported in Table 13. We also report the number of lines of each species that are measured in each star, and the error in the mean abundance.

For both the cluster IL and the individual stars, abundances relative to Fe are given using the solar abundance distribution of Asplund et al. (2005), with a solar $\log\epsilon(Fe) = 7.50$. The only exception is that we use the solar $\log\epsilon(O) = 8.93$ of Grevesse (1989). In the recent literature, we note that there has been a convergence of the solar oxygen abundance to a lower value, namely $\log\epsilon(O) = 8.66$ (Asplund et al. 2005). However, this value has not yet propagated into the Kurucz model atmosphere grids and so we are forced to adopt 8.93 dex in our calculations. Moreover, the results in the literature to which we compare our work have also used a higher value for all calculations and normalizations. For these reasons, we have elected to use the higher value for internal consistency in our analysis and with the literature. The abundance ratios for neutral species are reported with respect to $[Fe/H]_I$, and ionized species with respect to $[Fe/H]_{II}$.

In Figures 4 through 16, we show the LMC IL cluster abundances from our analysis (red squares) as a function of $[Fe/H]$ and age. The abundances measured in the individual stars are shown as black crosses. LMC abundances are shown with the MW IL GC training set abundances from Paper II (gray squares). For reference, we show a compilation of abundances measured for individual stars in the LMC as small red points and for the MW as small gray points. The small red and gray points that include error bars correspond to stellar abundances from clusters in the LMC and MW, respectively. References for individual star abundances are located in the captions of Figures 4 through 16. For the old sample of LMC clusters the error bars on the IL abundances in Figures 4 through 16 correspond to the standard error in the mean of the lines for each species. For the intermediate age and young clusters the error bar corresponds to σ_{Tot} , which includes the σ_{lines} and σ_{age} added in quadrature. For elements where only one clean line was measured, σ_{lines} was estimated using the χ^2 -minimization technique described in § 3.3.

5.1. Alpha Elements: Ca, Ti and Si

In this section, we present the abundances for α -elements Ca I, Ti I, Ti II and Si I. These are the first-ever α -element abundances for NGC 1916, NGC 1718, and NGC 1711. Abundances of O I and Mg I are discussed with the other light elements in §5.2. The abundances for all clusters are plotted in Figure 4 as a function of both $[Fe/H]$ (left panels) and age (right panels).

The $[Ca/Fe]$ for all clusters tends to decrease with decreasing age and increasing $[Fe/H]$, as one would expect. The old clusters (NGC 1916, NGC 2019, and NGC 2005) have $[Ca/Fe]$ in the range +0.2 to +0.4. The intermediate age clusters (NGC 1718 and NGC 1978) have $[Ca/Fe]$ of -0.14 and $+0.03$, respectively, from IL. Individual stars in NGC 1978 have $[Ca/Fe] = +0.10 \pm 0.13$. From both IL and individual star spectra, the youngest clusters (age < 1 Gyr) have a spread in $[Ca/Fe]$ between -0.19 and $+0.18$.

Our measurements, obtained by both IL and individual stellar spectra, agree with previous results (see detailed comparison in §6). While the abundance information available for the LMC is still limited, our results add to increasing evidence that there is generally a larger range in $[\alpha/Fe]$ in LMC stars than in MW stars of similar metallicity (e.g. Venn et al. 2004; Pritzl et al. 2005; Pompéia et al. 2008; Smith et al. 2002). This spread could indicate incomplete mixing of the LMC ISM, or possibly gas inflow or outflow.

In the data for this sample, there are more individual lines available for Ca I than for any other α -element. Therefore the Ca I measurements given here are the most statistically significant of our IL α -element results. While Ca is not a “pure” α -element — it is also produced in small quantities in Type Ia supernovae (SNe Ia) — it is the most accurate and consistent α -element for cluster comparisons. We find that the most evolution in $[Ca/Fe]$ occurs between 10 and 2 Gyrs ago, with a decreasing mean value over that range, and remains more or less constant since 2 Gyr ago. This implies that the LMC was dominated by SNe II enrichment early on, followed by significant SNe Ia enrichment before the second burst of star formation (~ 8 Gyr later) formed the intermediate age clusters (Harris & Zaritsky 2009). This is consistent with the evolutionary timescale for both SNe-types.

Our $[Si/Fe]$ measurements generally show the same behavior as our $[Ca/Fe]$ measurements: a spread in $[Si/Fe]$ for older clusters and decreasing $[Si/Fe]$ with decreasing age. Fewer Si I transitions make Si I more difficult to measure than Ca I. Nonetheless previous measurements of $[Si/Fe]$ in field and cluster stars in the LMC are consistent with our results, including some indication that mean values for $[Si/Fe]$ are ~ 0.1 - 0.2 dex higher than those of $[Ca/Fe]$, as can be seen in Figure 4.

In Figure 5, we show the results for Ti I and Ti II, separated by ionization state. $[Ti\ I/Fe]$ and $[Ti\ II/Fe]$ generally show both a larger line-to-line scatter and scatter between clusters than $[Ca/Fe]$ or $[Si/Fe]$, which is likely due to the S/N of the data. Despite the higher scatter, $[Ti\ I/Fe]$ and $[Ti\ II/Fe]$ are generally consistent with $[Ca/Fe]$ and $[Si/Fe]$ in that Ti decreases with decreasing age. Our $[Ti\ I/Fe]$ measurements are higher on average than previous measurements obtained for field and cluster stars, but the higher uncertainties in our measurements make

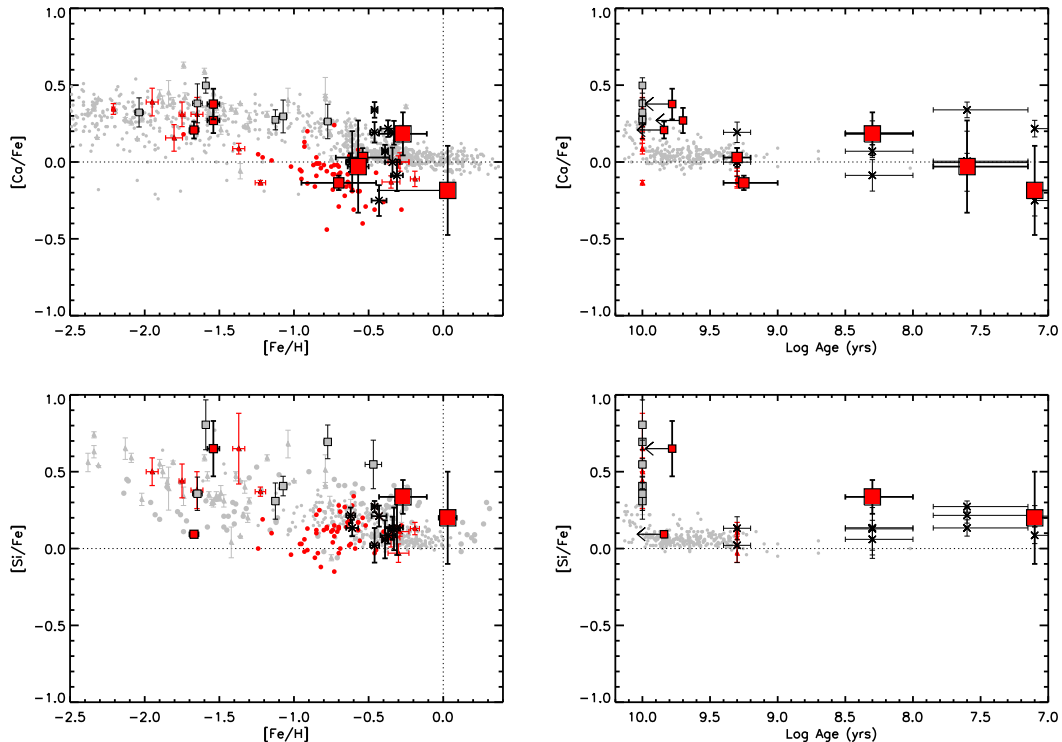


Figure 4. Left panels show Ca I and Si I ratios as a function of $[\text{Fe}/\text{H}]$, and right panels show the same as a function of age. Small, medium and large red squares show the old, intermediate, and young cluster LMC IL abundances, respectively. Large grey squares show the MW abundances from Paper II. Small black crosses show the individual stars in the young LMC clusters. Small grey and red points show MW and LMC stellar abundances from the literature. Data for MW stars are from Bensby et al. (2005), Venn et al. (2004), Pritzl et al. (2005) and references therein. For the LMC stars, triangles show abundances from J06, M08, M10, M11 and circles show abundances from P08. When possible the abundance ratios of other authors have been adjusted to be consistent with the solar abundance distribution of Asplund et al. (2005) that was used in our analysis. Ages for MW clusters and old LMC clusters are set to 10 Gyrs, and ages of LMC clusters of M08 are set to 2 Gyrs.

it difficult to determine if there is a systematic offset. Our $[\text{Ti II}/\text{Fe}]$ measurements overlap more with the field and cluster star measurements.

Although there is considerable scatter between clusters, we find that the mean $[\text{Ca}/\text{Fe}]$, $[\text{Si}/\text{Fe}]$, and $[\text{Ti}/\text{Fe}]$ for the old LMC clusters are consistent with measurements for MW clusters (e.g. Pritzl et al. 2005; Cameron 2009). This is further evidence that, like the MW, the LMC ISM was dominated by enrichment of SNe II when the old clusters formed ~ 10 Gyr ago. To clarify the overall trends, we have tabulated the mean $[\alpha/\text{Fe}]$ for the old LMC clusters in Table 14, and the mean $[\alpha/\text{Fe}]$ for the MW IL sample. This is particularly useful for comparisons with results in the literature from other abundance analysis techniques. The mean $[\alpha/\text{Fe}]$ for the old LMC clusters is only ~ 0.04 dex lower than for the MW training set GCs, and consistent within the statistical uncertainty. In Figure 6 we show the mean $[\alpha/\text{Fe}]$ as a function of $[\text{Fe}/\text{H}]$ for all of the LMC clusters, both old and young, as well as field stars in the MW and LMC.

5.2. Light Elements: O, Na, Mg, Al

It is well known that MW GCs exhibit star-to-star abundance variations for light elements involved in high temperature proton-capture nucleosynthesis (see Gratton et al. 2004, for a recent summary.). Recently, we found indirect evidence for abundance variations in M31 GCs (Colucci et al. 2009), and Mucciarelli et al. (2009) confirmed that abundance variations for O, Na,

Mg, and Al are also present in three old, metal-poor GCs in the LMC. This indicates that star-to-star abundance variations are likely to be ubiquitous and an integral part of massive cluster formation, not just limited to the MW. When star-to-star abundance variations are present, a fraction of stars in the cluster can exhibit any of the following to varying degrees: depleted O due to the ON-cycle, enriched Na due to the NeNa-cycle, and depleted Mg and/or enriched Al due to the MgAl-cycle. Recently, several authors have tried to connect these star-to-star abundance variations with the observations of multiple populations of stars in MW globular clusters (e.g. D’Ercole et al. 2008; Carretta et al. 2010; Decressin et al. 2007; de Mink et al. 2009; Conroy & Spergel 2011).

As mentioned above, we have already shown that indirect evidence for abundance variations can be measured in cluster IL spectra. Specifically, the IL analysis shows large scatter in $[\text{Mg}/\text{Fe}]$ when compared to other α -elements, as well as a lower mean $[\text{Mg}/\text{Fe}]$ and significantly elevated $[\text{Al}/\text{Fe}]$ and $[\text{Na}/\text{Fe}]$. This was seen both in our M31 GCs, mentioned above, and in Paper I and Paper II for the MW IL sample. The same indications of star-to-star abundance variations are now also clear in the IL of our old LMC clusters.

For all of our LMC clusters, the Na and Al abundances are shown in Figure 7, and the Mg and O abundances are shown in Figure 8. The old LMC clusters in our sample clearly have elevated $[\text{Na}/\text{Fe}]$ ($\sim +0.5$ dex) compared to

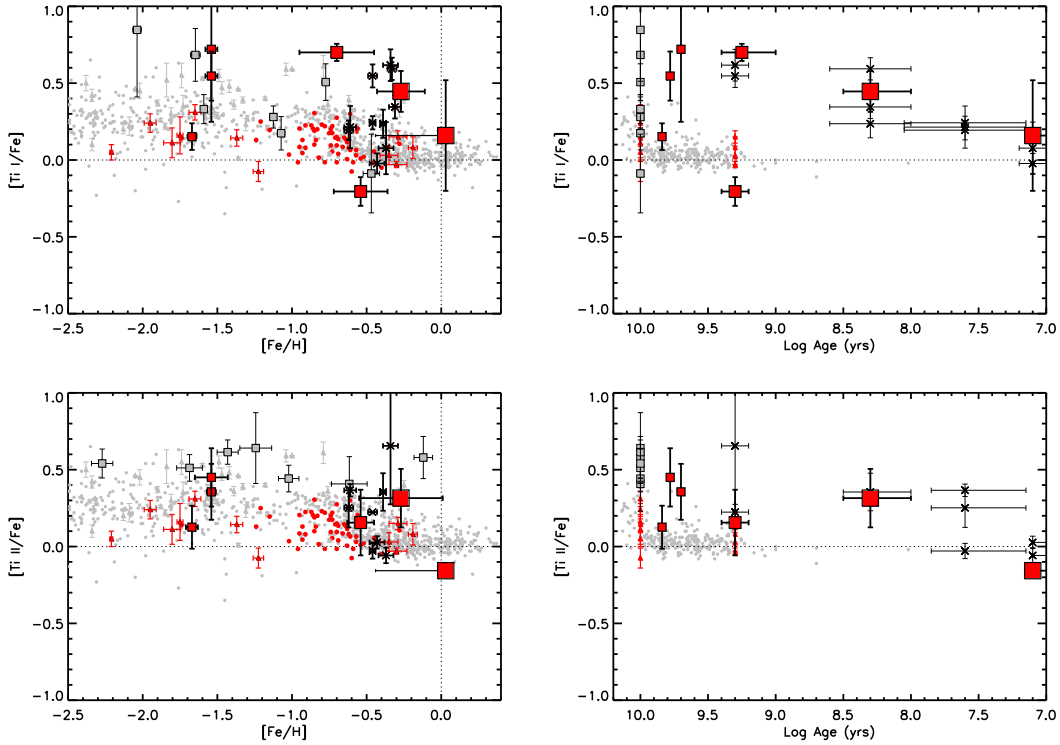


Figure 5. The same as Figure 4 for Ti I and Ti II.

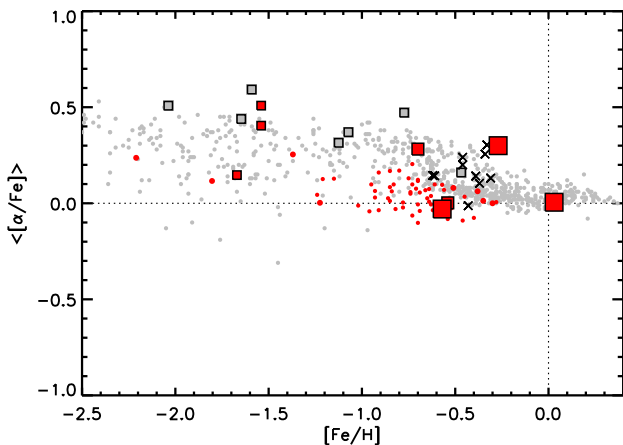


Figure 6. Mean $\langle [\alpha/Fe] \rangle$ calculated from Ca I, Ti I, Ti II, and Si I. Symbols and data for single stars are the same as in Figure 4.

field stars and younger clusters. The intermediate age clusters (NGC 1978 and NGC 1718) have significantly lower $[\text{Na}/\text{Fe}]$ with a wide range of values (~ -0.6 to $+0.1$). In the younger clusters, $[\text{Na}/\text{Fe}]$ is only available in the IL of NGC 1866, where $[\text{Na}/\text{Fe}] = +0.23 \pm 0.2$.

Because Na I is difficult to measure, it is worth noting the features from which our results are derived. The most accessible Na I features in cluster IL spectra are the 5682/5688 Å and 6154/6160 Å doublets, which are relatively weak ($\sim 30 \text{ m}\text{\AA}$), and so are measured with the line synthesis component of ILABUNDS. Stellar Na I abundances are measured with the SYNTH routine in MOOG. We have not corrected our cluster IL or stellar abundances for non-LTE effects, but note that for

cool giants ($T_{\text{eff}} < 5000 \text{ K}$) the corrections tabulated by Gratton et al. (1999) are at most +15 % at high metallicity.

The range in $[\text{Na}/\text{Fe}]$ found by Mucciarelli et al. (2009) is consistent with our result, as can be seen in Figure 7. Our measurements of $[\text{Na}/\text{Fe}]$ from 10 individual stars in the young clusters generally agree with the IL measurements, as can be seen in Figure 7.

Also in Figure 7 are our $[\text{Al}/\text{Fe}]$ results. Similar to $[\text{Na}/\text{Fe}]$, the old clusters clearly also have high $[\text{Al}/\text{Fe}]$, with a mean above $+0.5$ dex, as also true of some old MW clusters. The intermediate age clusters have $[\text{Al}/\text{Fe}]$ abundances similar to $[\text{Na}/\text{Fe}]$, with values significantly lower than for the old clusters. For young clusters, the IL and individual stars both show lower abundances than the intermediate age clusters. This results in a trend of decreasing $[\text{Al}/\text{Fe}]$ with decreasing cluster age, as can be seen in Figure 7. Like Na I, the Al I measurements come from line synthesis in both cluster IL and individual stars. All of our cluster IL abundances are obtained from the Al I 6696/6698 Å doublet, while the stellar Al I abundances are obtained both from the 6696/6698 Å doublet and the Al I 7835.31 Å feature.

Figure 8 shows the results for $[\text{Mg}/\text{Fe}]$. $[\text{Mg}/\text{Fe}]$ is generally consistent with other α -element abundances. Mean values for $[\text{Mg}/\text{Fe}]$ for the old clusters are in the range $+0.0$ to $+0.32$. We do not see evidence for significantly depleted $[\text{Mg}/\text{Fe}]$ with respect to $[\alpha/Fe]$ in the old clusters.

Over the full age range of the sample, $[\text{Mg}/\text{Fe}]$ generally decreases with decreasing cluster age. The only exception to this trend is NGC 1718, for which we obtain a significantly lower value of $[\text{Mg}/\text{Fe}] = -0.9 \pm 0.30$.

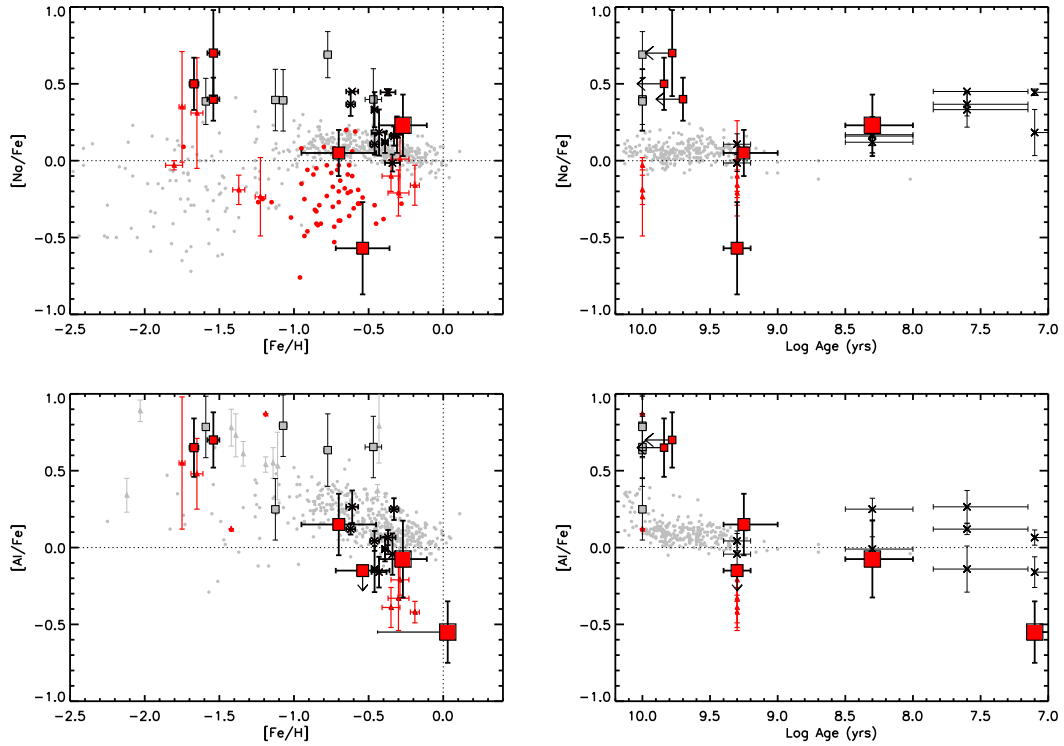


Figure 7. Same as Figure 4 for the light elements Al and Na. Symbols and data for single stars are the same as in Figure 4. Additional LMC individual star data (also triangles) are from Mucciarelli et al. (2009). Additional MW GC individual star data are from references compiled in Carretta (2006).

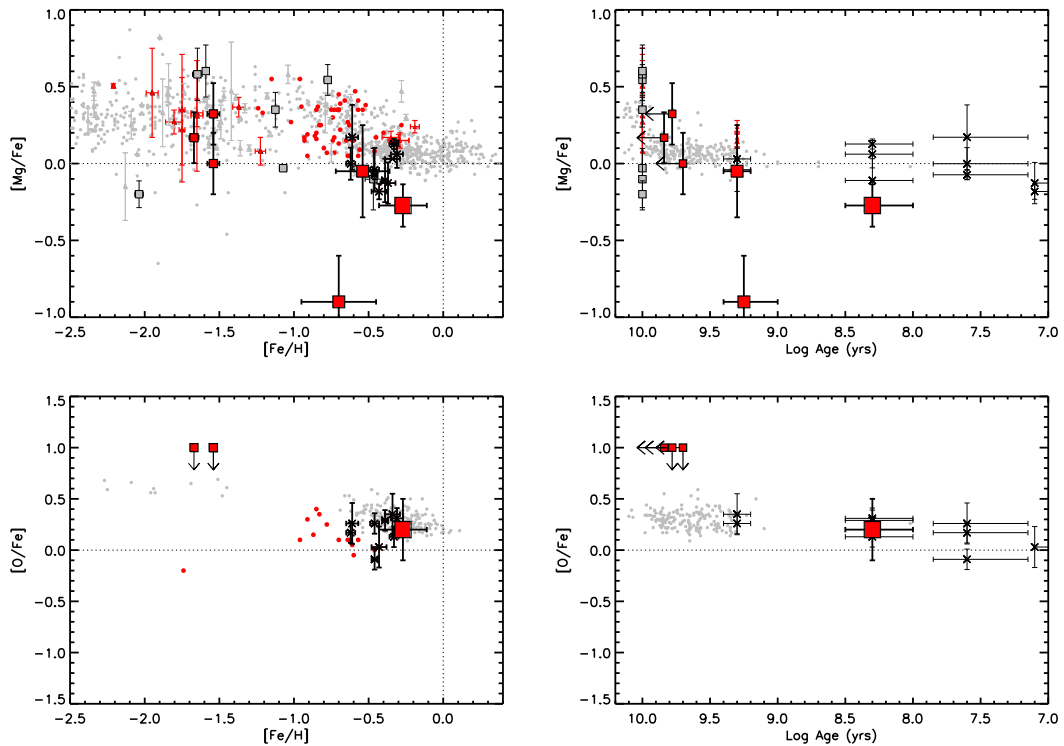


Figure 8. Same as Figure 4 for the light elements O and Mg. Symbols and data for single stars are the same as in Figure 4. Additional LMC individual star data (also triangles) are from Mucciarelli et al. (2009). Note that the cluster IL $[O/Fe]$ values are measured from the 7771 Å triplet, and that no non-LTE correction can currently be applied.

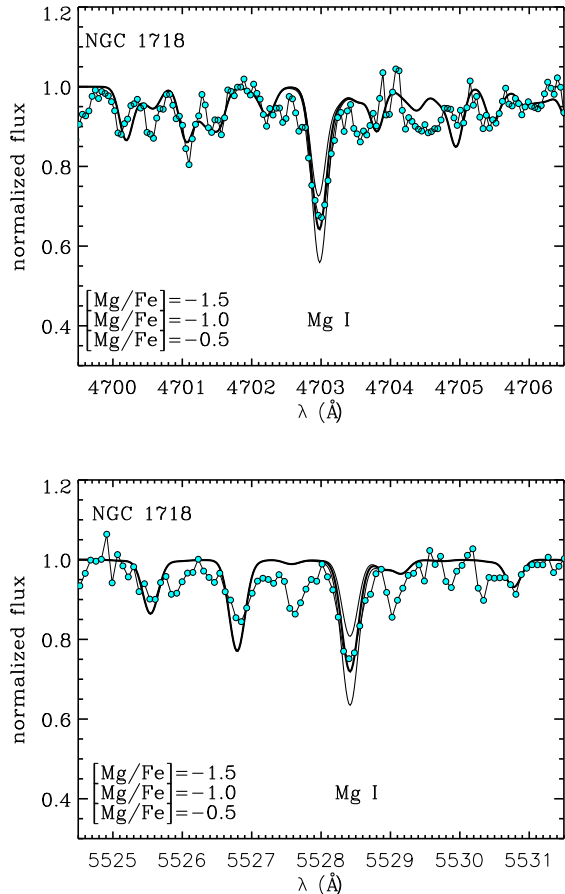


Figure 9. IL line syntheses for two Mg I features in the IL spectra of NGC 1718. Cyan circles show the data and thick black lines show syntheses of $[\text{Mg}/\text{Fe}] = -1.5, -1.0,$ and -0.5 . All synthesized spectra were created using a CMD with an age of 3 Gyr and a metallicity of $[\text{Fe}/\text{H}] = -0.73$, corresponding to our oldest acceptable solution for NGC 1718. Both the 4703 Å and 5528 Å features are best fit by the $[\text{Mg}/\text{Fe}] = -1.0$ synthesis.

The low Mg I in this cluster is interesting, although difficult to interpret. We note that this cluster has one of lowest masses in our sample. This may suggest that NGC 1718 formed in a poorly mixed environment in which high mass SNe II ($M > 35M_{\odot}$) had not contributed metals, as the highest mass SNe are thought to produce Mg and O most efficiently (Woosley & Weaver 1995). Our measurement appears robust because we obtain very similar abundances using spectral synthesis for two Mg I features which are separated in wavelength by ~ 1000 Å. This is shown in Figure 9, where we demonstrate that the best fitting syntheses have $[\text{Mg}/\text{Fe}] \sim -1.0$.

For the young clusters in our sample, we are able to measure Mg I in the cluster IL spectra of NGC 1866, and obtain $[\text{Mg}/\text{Fe}] = -0.27 \pm 0.2$. We obtain $[\text{Mg}/\text{Fe}] = -0.03 \pm 0.12$ from the individual stars in this cluster, which is consistent with the IL result, given the large uncertainties. From the individual stars in NGC 1711 and NGC 2100 we obtain $[\text{Mg}/\text{Fe}] = +0.08 \pm 0.08$ and -0.16 ± 0.04 , respectively. Previous measurements in individual stars (e.g. in NGC 1978) are consistent with our results and are discussed further in §6.

O I is always difficult to measure in cluster stars,

but is particularly difficult in the IL because of the velocity dispersion of the clusters (i.e. line broadening). Our IL estimates for O I are obtained by line synthesis of the 7771 Å triplet; the 6300 Å forbidden line is consistently too weak. For the old clusters, even the 7771 Å triplet is quite weak and we only obtain limits on O of $[\text{O}/\text{Fe}] < +1.0$ for NGC 2019, NGC 1916, and NGC 2005. For NGC 1866 (~ 100 Myrs) we measure $[\text{O}/\text{Fe}] = +0.2 \pm 0.3$. It is important to note that the 7771 Å triplet can have significant non-LTE effects in cool stars, which must be kept in mind when comparing to O abundances from the 6300 Å forbidden line. Unfortunately, there is no obvious way to correct the 7771 Å IL abundances for non-LTE effects, so we report the abundances with this caveat.

To these IL results, we can add several measurements from the stars in young clusters. The O I abundances for the individual stars were measured from the 6300 Å forbidden line. The stars in both the intermediate age and young clusters have a constant value of $[\text{O}/\text{Fe}] \sim +0.25$, similar to previous results for other LMC stars (P08; M11).

In summary, we find evidence for star-to-star abundance variations in the old clusters in our sample in the form of highly enriched $[\text{Na}/\text{Fe}]$ and $[\text{Al}/\text{Fe}]$. The $[\text{Mg}/\text{Fe}]$ and $[\text{O}/\text{Fe}]$ abundances are not indicative of star-to-star abundance variations on their own, but are still consistent with this picture. We find that $[\text{Na}/\text{Fe}]$, $[\text{Al}/\text{Fe}]$ and $[\text{Mg}/\text{Fe}]$ generally decrease with decreasing cluster age. In §7 we discuss the implications of our measurements further, including the dependence of the IL abundance with cluster mass.

5.3. Fe-peak Elements

Fe peak elements are well-studied in individual stars in the MW and LMC. In general, the abundances of Ni, Cr, Sc, V, and Co tend to scale with Fe, so that the $[\text{X}/\text{Fe}]$ ratios for these elements are approximately solar for $[\text{Fe}/\text{H}] > -2.0$, or occasionally sub-solar in the LMC (e.g. P08). The abundance of Mn, however, has a plateau value of $[\text{Mn}/\text{Fe}] \sim -0.4$ for $[\text{Fe}/\text{H}] < -1.0$, and then increases to solar ratios between $[\text{Fe}/\text{H}] = -1.0$ and $[\text{Fe}/\text{H}] = +0$.

We measure Ni I, Cr I, Sc II and V I in most of our LMC sample. We find that the abundance ratios for these elements are consistent with solar ratios across all of the ages and metallicities of the clusters, as shown in Figure 10. The scatter between cluster IL measurements is largest for Sc II, similar to what was found for IL measurements in the MW and in clusters in M31 (Cameron 2009; Colucci et al. 2009).

The Mn I abundances that we obtain for the LMC clusters are fairly constant, with a mean value of $[\text{Mn}/\text{Fe}] \sim -0.1$ dex, as shown in Figure 11. The older, lower metallicity clusters do not reach the MW low of $[\text{Mn}/\text{Fe}] \sim -0.4$. However, they do overlap with our MW IL measurements, so it is difficult to tell if the LMC ratios differ systematically.

The $[\text{Mn}/\text{Fe}]$ of the intermediate age and young clusters overlap with the higher metallicity MW field stars of Venn et al. (2004). For the youngest clusters we have only measured $[\text{Mn}/\text{Fe}]$ in the individual stars, and find that it is offset to lower ratios than MW field stars at

similar metallicities (see black crosses in Figure 11). We note that McWilliam et al. (2003) and Sbordone et al. (2007) found a similar pattern of low $[\text{Mn}/\text{Fe}]$ at high metallicity in the Sagittarius dwarf galaxy. To explain the observations in Sagittarius, McWilliam et al. (2003) and Cescutti et al. (2008) proposed that both metallicity dependent Mn-production in SNe II and SNe Ia as well as significant gas loss through galactic winds would be required. The gas-loss required in this case could also explain the reduced effective star formation rate between bursts that has been found for the LMC.

In Figure 11 we also show the $[\text{Co}/\text{Fe}]$ abundances. From the cluster IL we can measure Co I in one cluster, NGC 2019. The rest of the Co I abundances that we measure are obtained from the individual stars in the intermediate age and young clusters. We find $[\text{Co}/\text{Fe}]$ to be approximately solar in our sample. The abundances of P08, M08, and J06 are consistent with our results.

The last element shown in Figure 11 is Cu. Our $[\text{Cu}/\text{Fe}]$ ratios are significantly sub-solar (~ -0.9 dex) at all $[\text{Fe}/\text{H}]$. We are able to measure Cu I in the cluster IL spectra of NGC 1866. All of the other measurements we obtain for Cu I are from the individual stars in the intermediate age and young clusters. Previous measurements of $[\text{Cu}/\text{Fe}]$ by J06 and P08 are also sub-solar at both high and low metallicity, which is unlike the $[\text{Cu}/\text{Fe}] \sim 0$ ratios found in the MW for $[\text{Fe}/\text{H}] > -1$. Cu production is thought to occur in SNe II, and is metallicity dependent (e.g. Woosley & Weaver 1995; Bisterzo et al. 2005). As the abundance here is not seen to rise at any $[\text{Fe}/\text{H}]$, it appears that SNe II with higher $[\text{Fe}/\text{H}]$ are not impacting the overall metallicity of the LMC gas over time. This could be due to inflows of metal-poor gas, outflows of metal-rich gas, or low star formation rates over time with few high mass stars. Low $[\text{Cu}/\text{Fe}]$ was also measured for stars in the Sagittarius dwarf galaxy by McWilliam & Smecker-Hane (2005), where it was argued that this implied significant gas-loss after early generations of star formation.

In summary, most of the Fe-peak elements generally follow the abundance trends that have been previously measured in the LMC. We find depleted $[\text{Cu}/\text{Fe}]$ and $[\text{Mn}/\text{Fe}]$ at high metallicity, which may reflect the lower star formation efficiency of the LMC and metallicity-dependent SNe yields.

5.4. Neutron Capture Elements

The abundance ratios of neutron capture elements in different environments are particularly useful for constraining chemical evolution models, especially the contribution of AGB stars to the interstellar medium (Snedden et al. 2008). These elements have been observed to be critically sensitive to the star formation history of a galaxy and, like α -elements, show different patterns in dwarf galaxies than in the MW.

Many neutron capture elements have weak features in individual stellar spectra, and so are particularly difficult to measure in cluster IL. With EWs, we have been able to measure Ba II in most of the LMC clusters but can only measure Y II, Eu II, La II, Nd II, Sm II, and Sr II in 1–3 clusters each. Therefore, the line synthesis component of ILABUNDS was used to measure or put upper limits on these elements for most of the sample.

There is some scatter in abundance ratios for the light

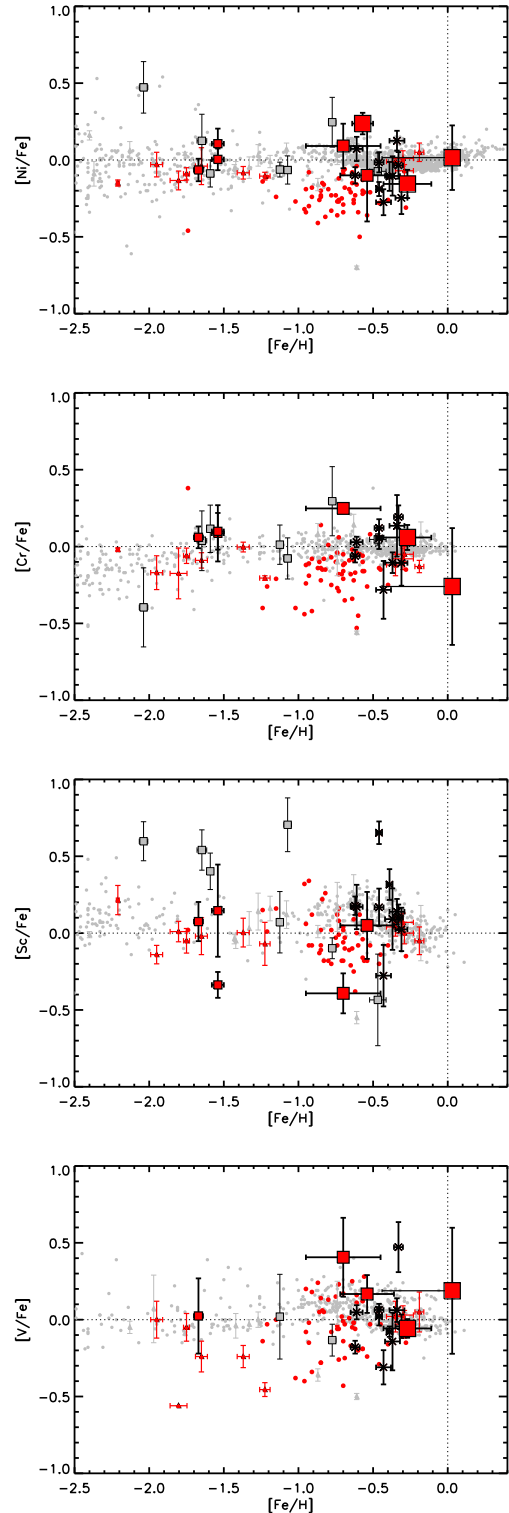


Figure 10. Abundances for Fe-peak elements Ni, Cr, Sc and V. Symbols are the same as in Figure 4.

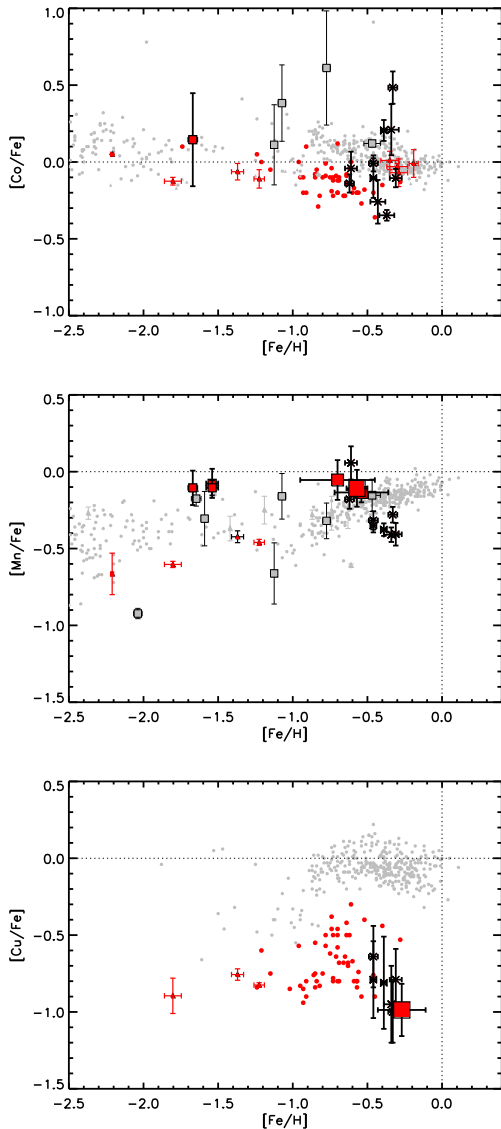


Figure 11. Same as Figure 10 for Co, Mn and Cu. Symbols are the same as in Figure 4.

s-process elements $[Y/Fe]$ and $[Sr/Fe]$ as shown in Figure 12 and 13. Sr II was measured in two old clusters; to our knowledge, these are the first Sr II measurements in LMC clusters to date. $[Sr/Fe]$ is sub-solar in both cases, and lower than both the IL MW measurement and the mean $[Sr/Fe]$ from LMC F-type supergiants (RB89).

From cluster IL, Y II measurements or upper limits were made for 6 of the 8 clusters. From the individual stars, we are able to measure both Y I and Y II in the intermediate age and young clusters. We find some scatter in $[Y/Fe]$ between clusters, and potentially some star-to-star scatter within some of the younger clusters, although our stellar samples in each cluster are small. In general, at high metallicity and young ages the results are consistent with solar ratios. We find similar $[Y/Fe]$ in the LMC clusters as we did for the MW clusters in Paper II.

In Figure 14, we show our measurements of $[Ba/Fe]$. $[Ba/Fe]$ is always super-solar in our sample, and the mean value is higher for the young and intermediate age clus-

ters than it is for the old clusters. The $[Ba/Fe]$ obtained from individual stars in younger clusters are also high: $[Ba/Fe] \sim +0.9$ dex. At low metallicity and older ages, the $[Ba/Fe]$ we obtain is consistent with previous stellar measurements in both the MW and the LMC. At high metallicity and younger ages, our measurements are similar to the high $[Ba/Fe]$ measured previously in the LMC (P08; M08; M11). High values of $[Ba/Fe]$ suggest that intermediate mass AGB stars had a significant effect on the chemical evolution of the LMC, which we discuss further in § 8.

We measure La II from cluster IL for NGC 2019, NGC 1978, and NGC 1866, as shown in Figure 15. The rest of our La II measurements are obtained from the individual stars in the younger clusters. We find $[La/Fe]$ to be approximately constant for all of the ages and metallicities in our sample, with a mean value of $[La/Fe] \sim +0.5$. The measurements of $[La/Fe]$ of P08 and M08 are consistent with our results.

As shown in Figure 15, we find more scatter in $[Nd/Fe]$ than we do for $[La/Fe]$, but the pattern of high ratios for all ages and metallicities is generally similar. From the individual stars in the youngest clusters, NGC 1711 and NGC 2100, there is some indication that the $[Nd/Fe]$ value decreased at late times in the LMC. High values of $[Nd/Fe]$ were also found in LMC clusters by J06; M08; M10, and in LMC field stars by H95. Nd II is obtained by line synthesis of the IL of four clusters, and by EW analysis for the individual stars.

Figure 16 shows some of the first Sm II measurements in the LMC, particularly for old stars. Although the sample is small, like $[La/Fe]$ and $[Nd/Fe]$, $[Sm/Fe]$ is relatively constant over the full age and metallicity range. There is little $[Sm/Fe]$ abundance information available for comparison, but LL92 and RB89 also found Sm to be overabundant in LMC supergiants by $\sim +0.4$ dex when compared to MW supergiants. Here we find evidence that this overabundance is also present at low metallicities and old ages.

In Figure 16 we show our $[Eu/Fe]$ abundances. We find $[Eu/Fe]$ to be consistently enhanced (~ 0.5 dex) over solar ratios for all of the clusters. Eu II abundances are obtained from line synthesis in both the cluster IL and the individual stars. These measurements are similar to what has been found for stars in other LMC clusters (J06; M08; M10). LL92 also find enhanced $[Eu/Fe]$ with respect to solar for very young LMC field stars, which is in contrast to the declining or solar $[Eu/Fe]$ found in MW stars of similar ages and metallicity.

In § 8 we discuss further implications of the LMC cluster neutron-capture abundances. We have demonstrated with the LMC cluster sample that many neutron-capture elements can be analyzed in high resolution IL spectra, and that this analysis method holds promise for strong constraints on these elements for distant, unresolved clusters.

6. ACCURACY OF LMC ANALYSIS: COMPARISON TO STELLAR RESULTS FROM THE LITERATURE

In §4 we demonstrated the accuracy of the IL analysis method with our own sample of individual stars in the youngest LMC clusters. In this section we further demonstrate the accuracy with abundances from individual stars in the literature.

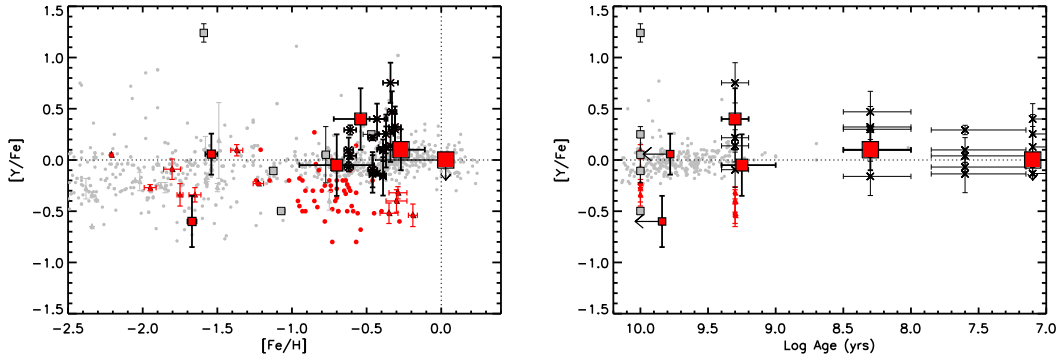


Figure 12. Same as Figure 4 for the neutron-capture element Y. For consistency with the Y II IL measurements, only the Y II stellar measurements are shown. Symbols are the same as in Figure 4.

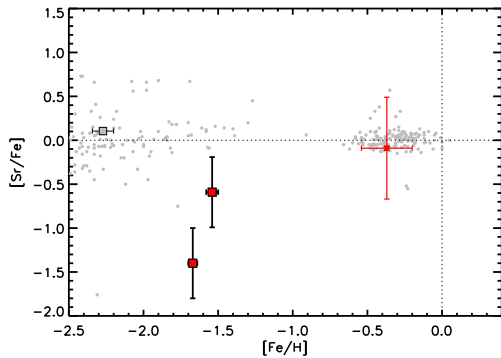


Figure 13. Abundances for the neutron-capture element Sr. The small red cross shows the mean $[\text{Sr}/\text{Fe}]$ of LMC F-type supergiants from RB89. Other symbols are the same as in Figure 4.

NGC 2019 and NGC 2005. The first comprehensive study of the detailed chemical composition in old LMC cluster stars was presented in J06. This work included three RGB stars in NGC 2019 and three in NGC 2005. As discussed in Paper III, we find the $[\text{Fe}/\text{H}]$ for NGC 2019 is lower by ~ 0.3 dex than in J06, and higher for NGC 2005 by ~ 0.25 dex.

As for the rest of the elements, we illustrate a comparison of the $[\text{X}/\text{Fe}]$ values for the two analyses of NGC 2019 in Figure 17. This comparison is similar to that described in §4; perfect agreement corresponds to the solid black 1:1 line, and we identify a small systematic offset with a linear least squares fit. The uncertainties in the measurements are shown by the vertical error bars, which correspond to the error in the mean of the abundance of each element ($\sigma/\sqrt{N_{\text{lines}} - 1}$). We note that the abundances from J06 come from a small sample of 3 stars, which have uncertainties comparable to the IL uncertainties due to the difficulty in obtaining high S/N stellar spectra in the LMC. The points in Figure 17 therefore have horizontal error bars corresponding to the error in the mean abundance for each species from J06. We have removed the light elements Na, Al, and Mg from the fit because we do not expect them to track the measurements of J06 if star-to-star abundance variations are present (see § 5.2).

From the dashed line in the top panel of Figure 17, we see that for NGC 2019, the abundance ratios are very consistent, and the systematic offsets in neutral and ionized species are small (< 0.1 dex). Therefore, the overall

abundance distribution pattern derived for NGC 2019 is very similar for the two analyses. The outliers in the comparison are $[\text{Si}/\text{Fe}]$ and $[\text{Y}/\text{Fe}]$. This is probably because the dispersion in Si between the 2 stars of J06 is large, and that Y II is very difficult to measure.

Due to lower S/N of our IL spectra of NGC 2005, we were only able to measure abundances for 10 elements. As for NGC 2019, we remove the light elements Mg and Na from the comparison for NGC 2005. When we compare the remaining elements to those of J06, we find a positive offset for the neutral and ionized species of $\sim +0.3$ dex, just as we found for Fe in Paper III. When this offset is accounted for, the abundance ratios agree very well, as can be seen in the residual plot of Figure 18. The exception is $[\text{Mn}/\text{Fe}]$, which may be systematically high for all three old clusters (see § 5.3).

NGC 1978. While we have already discussed a detailed comparison of stellar and IL analyses of our own analyses of NGC 1978 in §4, it is also interesting to compare our results to the recent work of M08 and Ferraro et al. (2006), who presented the abundances of ~ 20 different elements for a sample of 11 stars.

We compare the $[\text{X}/\text{Fe}]$ of our IL analysis to the stellar sample of M08 in Figure 19. We find a small, ~ -0.1 dex offset in neutral species, and a large positive offset in ionized species, although the dispersion is large ~ 0.4 . The scatter is consistent with what we find from the comparison to our own stellar analysis in §4, and is likely driven by the unavoidably poorer data quality of the IL spectra of NGC 1978.

NGC 1866. Like NGC 1978, for NGC 1866 we have already demonstrated good agreement between IL analysis and stellar analysis for our own sample. Here, we also compare our IL analysis to the stellar sample of M11, as shown in Figure 20. We find a small $\sim +0.1$ dex offset in the neutral species, and a larger offset of $\sim +0.4$ dex in the ionized species. As for the other clusters in our sample, when these offsets are removed the abundance pattern is very similar in both analyses. The remaining outlier is $[\text{Cu}/\text{Fe}]$, which is one of the more uncertain measurements because it is obtained from a single line.

NGC 2100. Using medium resolution spectra, Jasniewicz & Thevenin (1994) estimated Ca, Ti, Cr and Fe for NGC 2100. Their estimates for $[\text{Ca}/\text{Fe}]$, $[\text{Ti}/\text{Fe}]$ and $[\text{Cr}/\text{Fe}]$ are consistent with our measurements obtained with high resolution spectra.

In conclusion, as expected, we find minor systematic

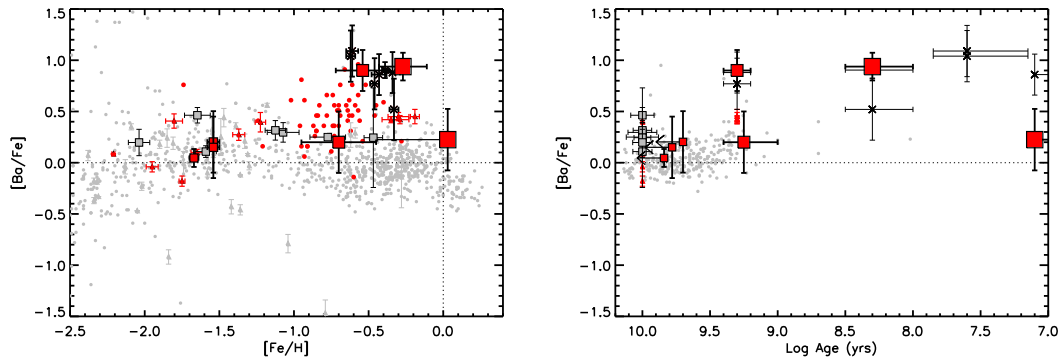


Figure 14. Same as Figure 4 for the neutron-capture element Ba. Symbols are the same as in Figure 4.

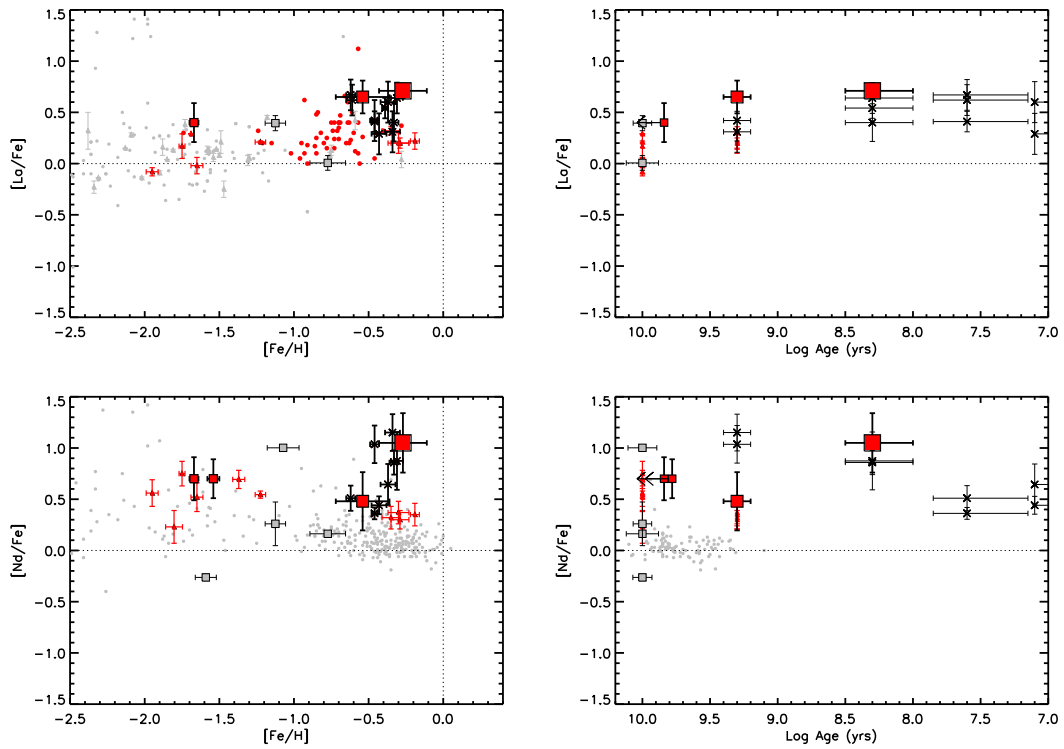


Figure 15. Same as Figure 4 for the neutron-capture elements La and Nd. Symbols are the same as in Figure 4.

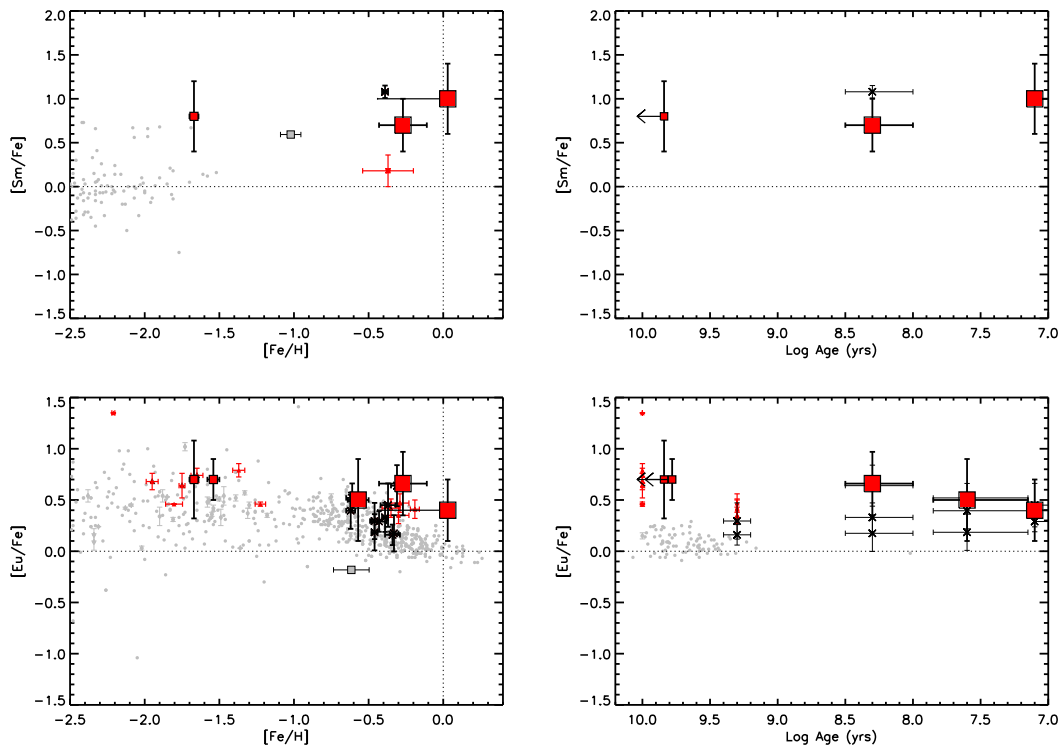


Figure 16. Same as Figure 4 for the neutron-capture elements Sm and Eu. Small red cross shows the mean [Sm/Fe] of LMC F-type supergiants from RB89. Other symbols are the same as in Figure 4.

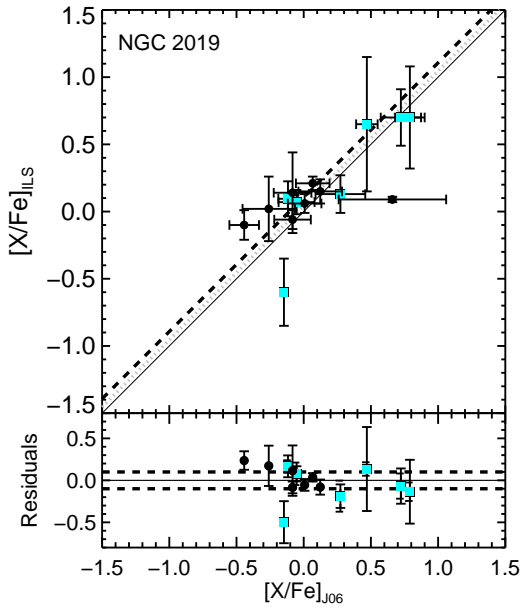


Figure 17. Comparison of abundance ratios from IL and stellar analysis for NGC 2019. Stellar abundances are from J06. Black and cyan points show abundances for neutral and ionized species, respectively. Solid line shows the 1:1 line where points would lie if there were perfect agreement between IL and stellar results. Dashed and dotted lines show linear fits to the neutral and ionized species, with the slopes constrained to unity. Bottom panel shows the residuals from the linear fit. The dashed lines correspond to residuals of ± 0.1 dex to guide the eye.

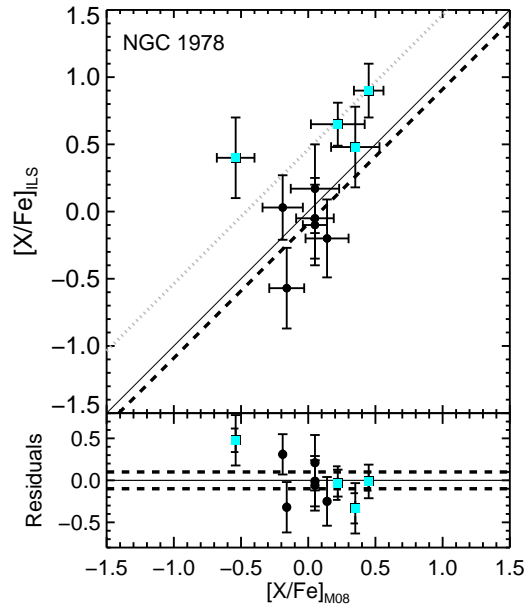


Figure 19. Same as Figure 17 for NGC 1978. Stellar abundances are from M08.

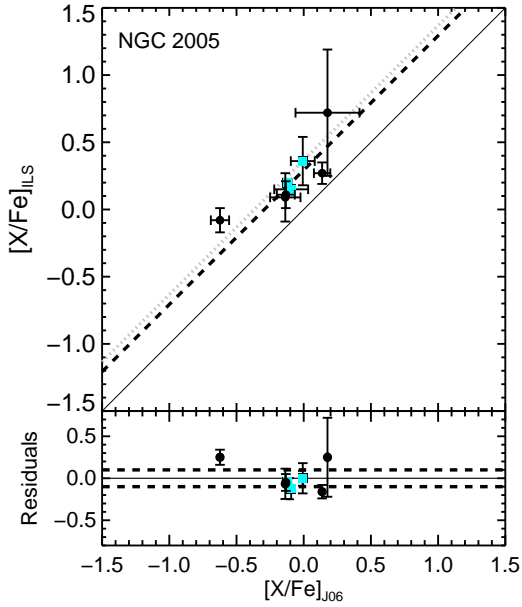


Figure 18. Same as Figure 17 for NGC 2005. Stellar abundances are from J06.

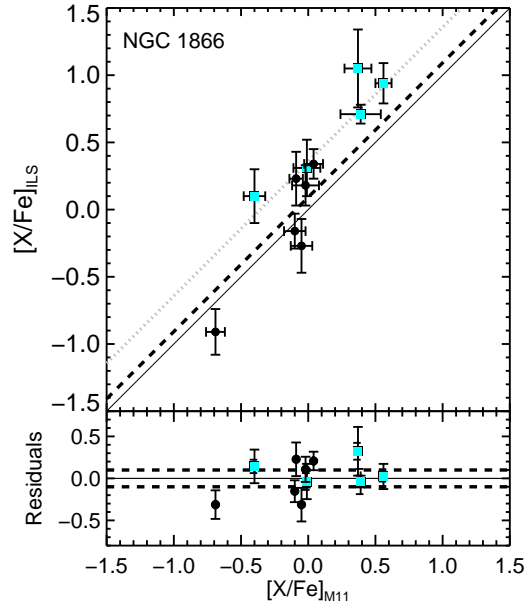


Figure 20. Same as Figure 17 for NGC 1866. Stellar abundances are from M11.

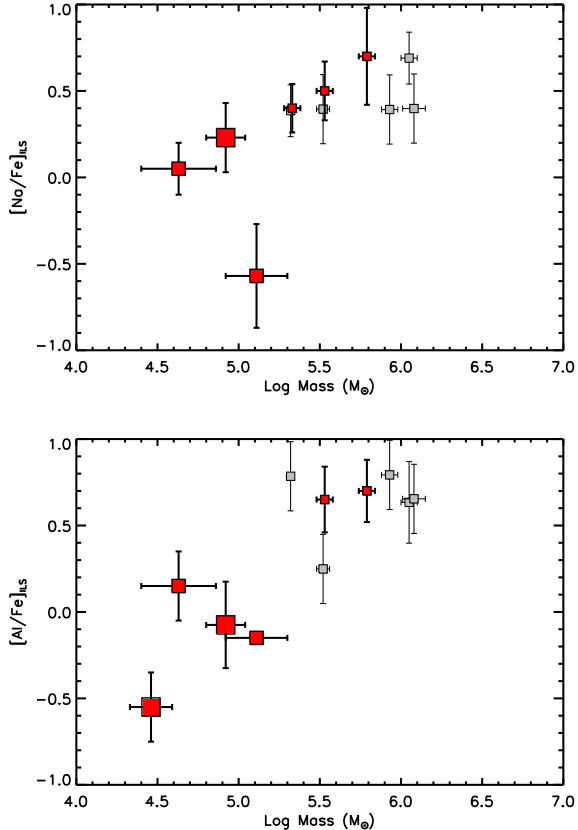


Figure 21. The dependence of integrated light element abundances on total cluster dynamical mass. The symbols are the same as in Figure 4. All cluster masses are taken from McLaughlin & van der Marel (2005), with the exceptions of NGC 6397, NGC 6752, and NGC 1978, which are taken from Drukier (1995), Baumgardt & Makino (2003), and Meylan et al. (1991), respectively.

offsets in our IL detailed abundance measurements when compared with previous stellar measurements by other authors. However, when these offsets are accounted for, we find that the abundance patterns of the clusters, as traced by the $[X/Fe]$ ratios, are very consistent using both stellar and IL techniques.

7. CLUSTER FORMATION AND LIGHT ELEMENTS

As presented in §5.2, we have measured enhanced Al and enhanced Na in the IL spectra for the old clusters the LMC. These results imply that these clusters have star-to-star abundance variations in the light elements that are sensitive to proton-capture nucleosynthesis. No previous work has obtained enough stars in these clusters to address this issue.

It is interesting to discuss our results in the context of recent theoretical works that aim to connect cluster star-to-star abundance variations with the multiple stellar populations that have been observed in old and intermediate age clusters (e.g. Piotto et al. 2007; Mackey et al. 2008; Milone et al. 2009; Goudfrooij et al. 2011). One scenario is that a second generation of cluster stars forms out of material that has been polluted with hot bottom burning products from the first generation intermediate mass ($4 - 8M_{\odot}$) AGB stars. Using this framework, Conroy (2011) find a correlation between total cluster mass and the fraction of current cluster mass that was

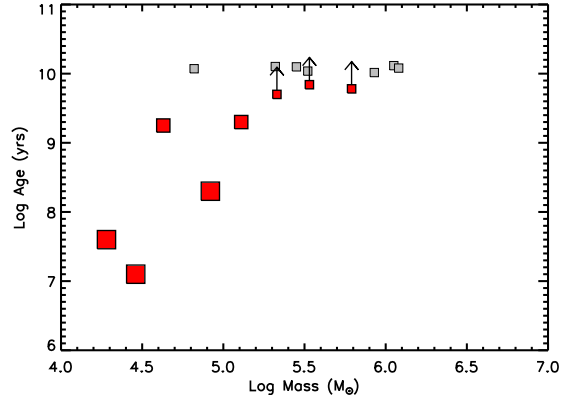


Figure 22. The relationship between cluster age and cluster mass. The symbols are the same as in Figure 4. LMC cluster ages are taken from Paper III, and all MW cluster ages are from Marín-Franch et al. (2009).

formed out of pure AGB star ejecta. Conroy (2011) obtain this result by parametrizing the observed Na-O correlations in MW clusters, but also find consistency with the observations of LMC intermediate age clusters of M08.

We find a correlation, with some scatter, of Na and Al abundances with cluster mass, as shown in Figure 21. This is consistent with a scenario where more massive clusters have a higher fraction of stars that are composed of pure AGB ejecta, as discussed in Conroy (2011). The trends are related to the trends of decreasing Na and Al with cluster age that were discussed in §5.2, because the younger LMC clusters have smaller masses, as shown in Figure 22. However, we note that there would not be high $[Na/Fe]$ and $[Al/Fe]$, and thus no trend with mass, if star-to-star abundance variations were not present in the old clusters in the sample. The trend for the intermediate age clusters is more ambiguous because of the mass-age relationship of our current sample. We note that Conroy (2011) find that the stars in NGC 1978 (age ~ 2 Gyr) that were observed by M08 show a weak but detectable Na-O correlation (and thus star-to-star abundance variations), which is consistent with our result for clusters in this age range.

It is interesting to look for star-to-star abundance variations in the young clusters because the pollution timescale ($\sim 10^8$ yrs) for the first generation of stars is thought to be comparable to the ages of some of these clusters (e.g. Conroy & Spergel 2011; de Mink et al. 2009; Decressin et al. 2007; D’Antona & Ventura 2007). Strong constraints on this timescale come from observations of age spreads of $\sim 10^8$ years at the main sequence turnoffs in some ~ 2 Gyr age LMC clusters (Milone et al. 2009; Goudfrooij et al. 2011). Like the intermediate age clusters, the youngest clusters in our sample have Na and Al ratios that are similar to what a pristine first generation of stars should have (Conroy 2011). These ratios and the mass-age relationship make it difficult, if not impossible, to determine if star-to-star abundance variations are present in the cluster by using the integrated light. We note that M11, with a large sample of individual stars in NGC 1866, claim that there is no evidence for star-to-star abundance variations in this cluster (age ~ 150 Myr). Unfortunately, the numbers of individual

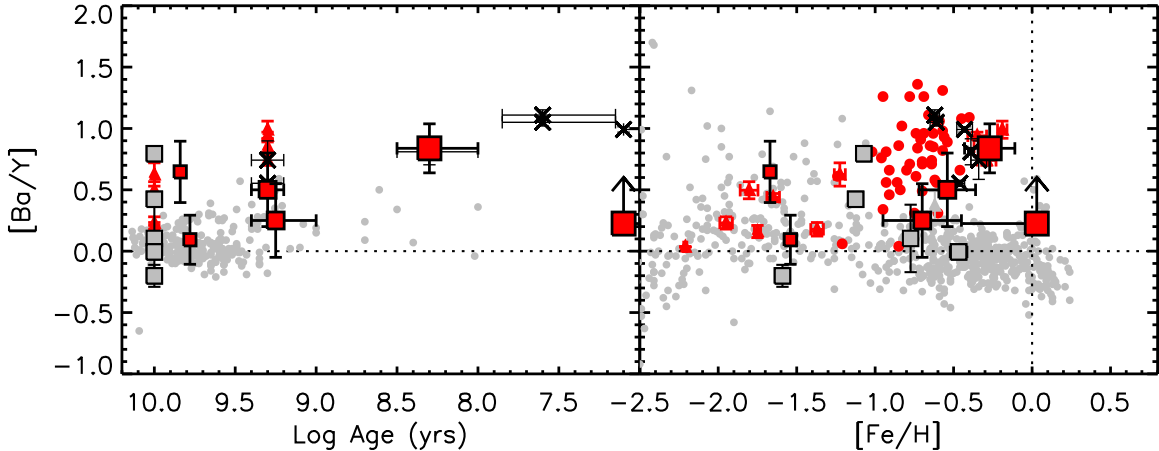


Figure 23. The ratio of heavy to light s -process elements ($[\text{Ba}/\text{Y}]$) as a function of age and $[\text{Fe}/\text{H}]$. Symbols are the same as in Figure 4.

stars that we have observed in each cluster in our sample are too small to determine if star-to-star variations are present. Therefore we conclude that our present data do not allow us to definitively answer the question of whether star-to-star abundance variations are present in massive clusters with ages of $\lesssim 100$ Myrs.

8. GALAXY FORMATION AND HEAVY ELEMENTS

As discussed in §5.4, we have measured many of the first abundances of 7 neutron-capture elements (Sr, Y, Ba, La, Nd, Sm, Eu) in these LMC clusters. Relative to Fe, the most notable results in our sample are that Ba, La, Nd, Sm, and Eu are significantly enhanced in the young clusters. While enhanced heavy element abundances have been found in young LMC stars for many years (Russell & Bessell 1989; Luck & Lambert 1992; Spite et al. 1993), this is the first indication that these elements are also enhanced in clusters with ages < 300 Myrs.

Neutron capture elements are generally divided into r - and s -process categories based on the neutron density of the site that dominates their production. However both high density, rapid-neutron capture (r -process) sites and lower density, slow-neutron capture (s -process) sites can both contribute to the overall abundance of heavy elements over time. For example, while Eu is often referred to as an r -process element because 97% of the Eu in the Sun was produced in the r -process, a larger fraction of Eu could come from s -process sites in an environment with a different (e.g. slower) star formation history. To better constrain the star formation history of a population, it is therefore useful to look at the ratios of different heavy elements to each other, rather than just to Fe in order to disentangle the relative dominance of s - and r -process sites. In addition, the relative abundances of s -process light (Sr, Y) and heavy (Ba, La) peaks can provide interesting constraints on the relative contributions of metal-poor and metal-rich AGB stars, because light s -process elements are produced less in low metallicity AGB stars (Busso et al. 1999; Sneden et al. 2008). This is because at low metallicity the lighter s -process element production is bypassed because the neutron flux per seed Fe nuclei is higher than at high metallicity when more

Fe nuclei are present.

The ratio $[\text{Ba}/\text{Y}]$ is a convenient diagnostic of the s -process in this way. In the MW, $[\text{Ba}/\text{Y}]$ is fairly constant over all ages and $[\text{Fe}/\text{H}]$ values, implying a high star formation rate at early times, and that heavy and light s -process elements were produced in similar amounts at all times (i.e. by high metallicity AGB stars). In the LMC, we find that the young clusters in our sample have $[\text{Ba}/\text{Y}] > +0.5$, as shown in Figure 23. This high $[\text{Ba}/\text{Y}]$ result implies that low metallicity AGB stars dominated the s -process yields over a long range in $[\text{Fe}/\text{H}]$ — the star formation rate was low at early times and metallicity increased slowly.

Because high-metallicity AGB stars produce heavy and light s -process elements in similar amounts, the imprint of low star formation rate at early times (high $[\text{Ba}/\text{Y}]$) will remain in younger, metal rich stars. In the LMC, high $[\text{Ba}/\text{Y}]$ at *any* $[\text{Fe}/\text{H}]$ therefore demonstrates that it had a low star formation rate at early times. The fact that $[\text{Ba}/\text{Y}]$ seems to increase in the LMC with increasing $[\text{Fe}/\text{H}]$ and decreasing age further implies that low metallicity AGB stars have contributed significantly to the cluster-forming gas at late times as well. This proves that the LMC has undergone much slower star formation than the MW, even though we see evidence of recent star-bursting episodes. In general, this is consistent with the evidence from Cu and Mn (see §5.3) that the LMC may have experienced a significant reduction in overall metallicity due to outflows of metal-rich gas, or inflows of metal-poor gas.

The old clusters in our sample have low $[\text{Ba}/\text{Eu}]$ and $[\text{La}/\text{Eu}]$, shown in Figure 24. This is indicative of neutron-capture element enrichment dominated by the r -process (Arlandini et al. 1999; Simmerer et al. 2004) at early times, similar to the MW halo. This is compatible with our results for α -element enrichment in the old clusters, because the r -process and α -element production are both thought to occur in SNe II. The intermediate-age and young clusters, particularly the individual member stars, have higher $[\text{Ba}/\text{Eu}]$ and $[\text{La}/\text{Eu}]$ than the old clusters, which reflects the contribution of s -process products at higher metallicity and later times.

In Figure 25, we show the ratio of r -process elements

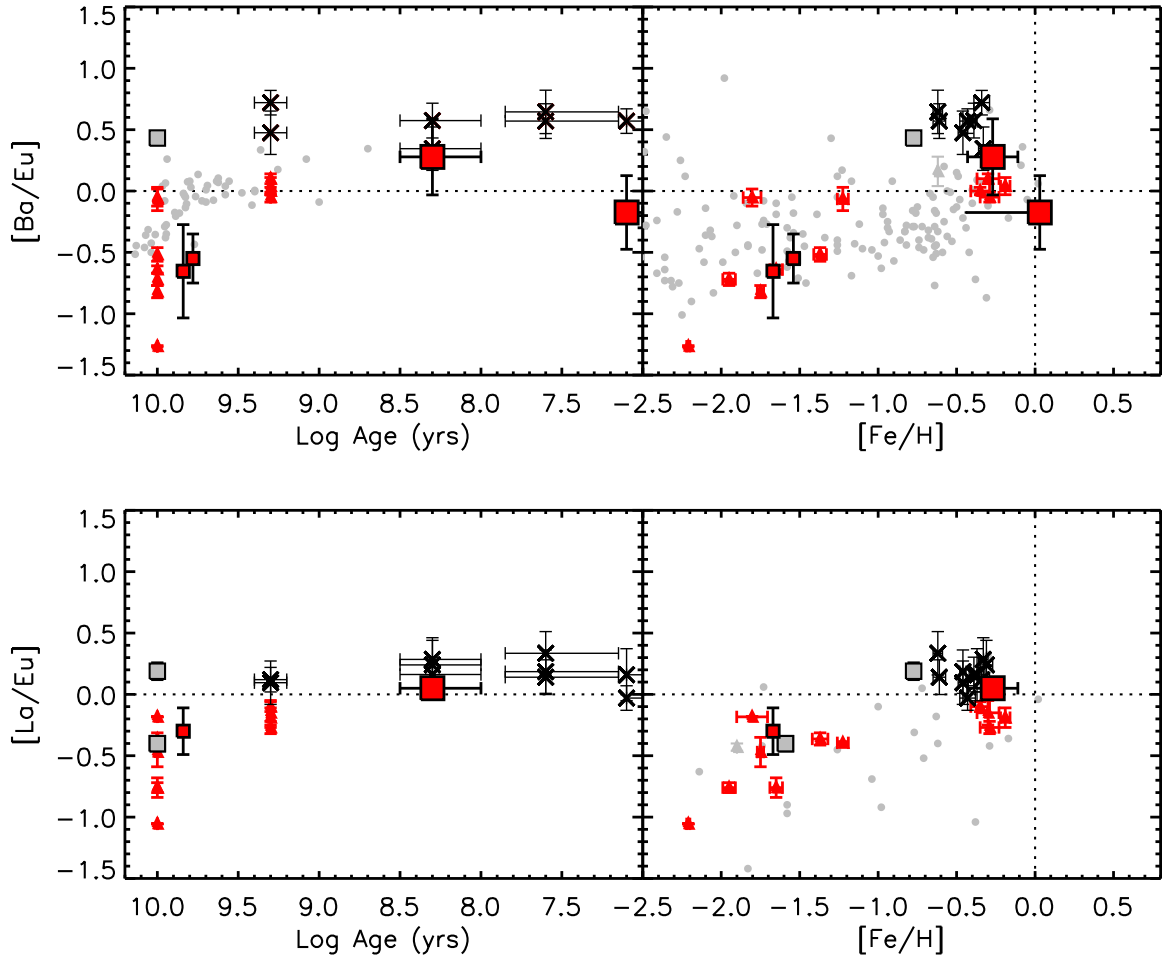


Figure 24. Top panels show the ratios of heavy s -process to r -process, $[Ba/Eu]$, as a function of age and $[Fe/H]$. Bottom panels show the ratio of heavy s -process to r -process elements $[La/Eu]$. Symbols are the same as in Figure 4.

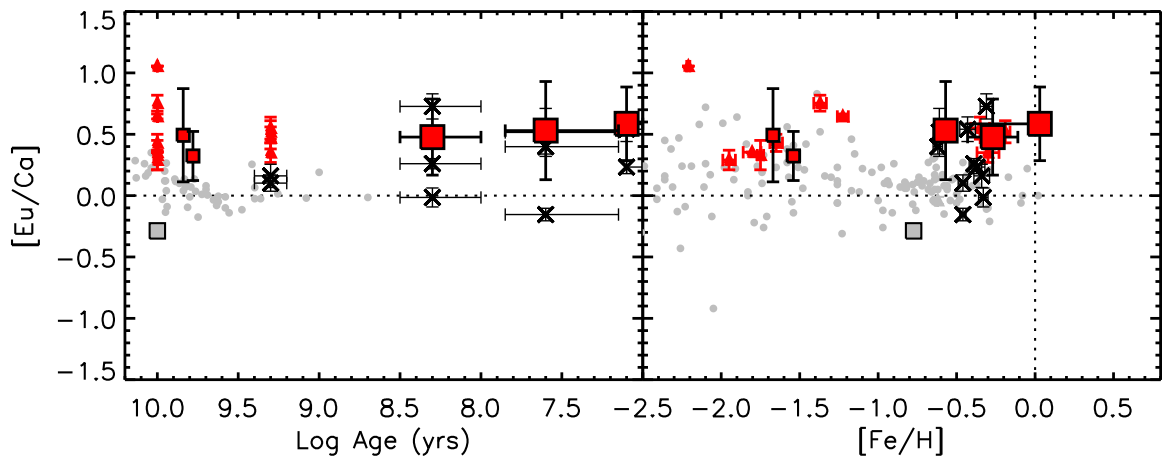


Figure 25. The ratios of r -process elements to α -elements ($[Eu/Ca]$) as a function of age and $[Fe/H]$. Symbols are the same as in Figure 4.

to α -elements, represented by [Eu/Ca]. The ratios of these two groups of elements are interesting because they both are in large quantities in SNe II. We observe [Eu/Ca] $\sim +0.5$ for all clusters, which is consistent with previous work on LMC clusters (M08; M10). The enhanced [Eu/Ca] are interesting for two reasons. The first is that all of the older clusters at the lowest metallicities observed in the LMC studied thus far show enhanced [Eu/Ca], while in the MW there is a lot of scatter in this ratio at lower metallicities. This scatter in the MW [Eu/ α] abundances is believed to be evidence that not all SNe II produce the same amount of r -process products, while they do seem to produce very consistent amounts of α -elements (Snedden et al. 2008). M10 concluded that consistently high [Eu/ α] at low metallicity implies an unusually efficient r -process in the LMC relative to the MW. The second reason is that Eu abundances are enhanced relative to Ca and Fe at high metallicity and young age. This may be a result of the second burst of star formation and corresponding increase in SNe II and r -process products that kept [Eu/Fe] elevated. However, it is also possible that a significant contribution to the Eu abundance comes from s -process sites, especially at young age and high metallicity. This would be consistent with the overall dominance of s -process production of Ba, La, and Nd that is clear from the ratios of these elements to Eu, as discussed above. Our data do not conclusively distinguish between these alternatives.

9. COMPARISON WITH A BASIC DUAL-BURST MODEL

With our sample of clusters we can probe the chemical evolution of the LMC in a self-consistent way over a larger range in age and [Fe/H] than has been possible before. In Figure 26 we compare the LMC training set abundances to the analytical chemical evolution model for the LMC by Pagel & Tautvaisiene (1998). The model assumes supernova yields and time delays identical to models for the solar neighborhood, and employs bursting star formation rates, infall, and galactic winds to match the age and [Fe/H] data for the LMC that was available at the time. As seen in the age-[Fe/H] plot in Figure 26, the model is a reasonably good fit to the age-[Fe/H] relationship for the LMC training set clusters, as well as the cluster samples of J06, M08, M10, and M11.

Our IL analysis now provides information on [X/Fe] ratios covering the same dynamic range in age as the well-established LMC age-[Fe/H] relationship. At the time, Pagel & Tautvaisiene (1998) could only compare their models with abundances from young LMC supergiants, and so they only had power to constrain their models in [X/Fe] and [Fe/H] space. In general, Pagel & Tautvaisiene (1998) found reasonable agreement, but noted that there was a large scatter in supergiant abundances, and it was unclear if the scatter was real or due to measurement uncertainties. We can now test the model of Pagel & Tautvaisiene (1998) with elements other than Fe, with finer age resolution than is possible for individual field stars. In Figure 26, we show examples for [Ca/H], [Eu/Fe] and [Ca/Fe] as a function of age. The agreement for age and [Ca/H] or [Ca/Fe] is generally good and similar to the good agreement for age and [Fe/H]. However, agreement is poorer for [Eu/Fe]. In general, the model is offset to lower abundances, which could mean that the overall supernova yields assumed are

too low. However, even if we applied a positive offset to the model, it would still fail to produce the high [Eu/Fe] found at the youngest ages in the LMC.

Our abundance data provides unprecedented constraints that are needed for tests of new chemical evolution models for the LMC. In future work we will investigate models for the chemical evolution of the LMC, focussing on the parameter space that is consistent with the age-[X/Fe] relationships for all ~ 20 elements that we have obtained in this work.

10. SUMMARY

We have presented chemical abundances of ~ 20 elements in 8 clusters in the LMC. These clusters have ages of 0.05 to 12 Gyrs and $-1.7 < [\text{Fe}/\text{H}] < +0.0$. Abundances were primarily measured by fitting individual absorption line EWs. For absorption lines that were too weak or too low S/N to measure with EWs, we developed an additional technique using a χ^2 -minimization scheme for IL synthesized spectra. In addition to the cluster IL abundances, we have also obtained abundances for 10 individual stars in the youngest clusters in our sample. The new results found in this work can be summarized as follows:

- We verify that the IL method provides [X/Fe] accurate to $\lesssim 0.1$ dex in clusters with ages < 2 Gyr.
- We provide the first detailed chemical abundances for 18 elements in the old cluster NGC 1916, for 12 elements in the intermediate age cluster NGC 1718, for 22 elements in the young cluster NGC 1711, and for 19 elements in the young cluster NGC 2100.
- We obtain the first measurements of Sr II in old LMC stellar populations, with the result that [Sr/Fe] is sub-solar in the old LMC clusters of our sample.
- We obtain the first measurements of Sm II in old LMC stellar populations, with the result that [Sm/Fe] is super-solar for the three clusters in our sample in which it was measured.
- We find evidence of a spread in α -enhancement at old age and similar [Fe/H] (NGC 2019 and NGC 1916), which implies that ISM in the LMC was not well-mixed at the time these old clusters formed.
- We find evolution in [α /Fe] with age and [Fe/H] in the LMC. This reflects the growing contribution of SNe Ia enrichment products in the LMC between 10 and 2 Gyr ago.
- We measure elevated [Na/Fe] and [Al/Fe] in our sample of old clusters, including the first evidence that NGC 1916, NGC 2019, and NGC 2005 harbor star-to-star abundance variations.
- We find decreasing [Na/Fe], and [Al/Fe] with decreasing cluster age and decreasing cluster mass, which could mean that the fraction of pure AGB ejecta incorporated into second generation stars is dependent on the total cluster mass.

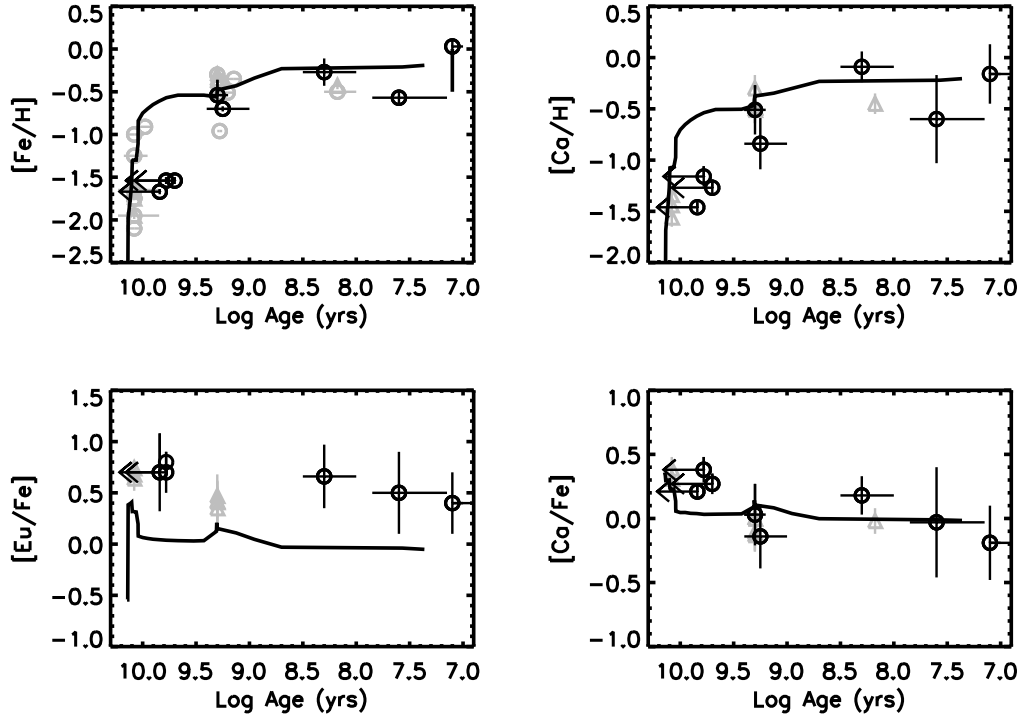


Figure 26. LMC age and abundance relationships for $[\text{Fe}/\text{H}]$, $[\text{Ca}/\text{H}]$, $[\text{Eu}/\text{Fe}]$, and $[\text{Co}/\text{Fe}]$. Our IL LMC cluster data are plotted as black circles. Gray circles are cluster abundances from J06, M08, M10, and M11. Black lines show the analytical chemical evolution models of Pagel & Tautvaišienė (1998) for the LMC.

- We find low $[\text{Mn}/\text{Fe}]$ and $[\text{Cu}/\text{Fe}]$ at high metallicity and young age in the cluster sample. This could reflect the low star formation efficiency of the LMC and possibly metal-rich outflows of gas.
- We obtain elevated La, Nd, Sm, and Eu ratios for all of the clusters in our sample.
- We obtain increasing $[\text{Ba}/\text{Fe}]$ and $[\text{Ba}/\text{Y}]$ with decreasing cluster age, which is evidence that there has been significant contributions to the LMC ISM of ejecta from low-metallicity AGB stars throughout the history of the LMC. This is consistent with prolonged or low efficiency star formation in the LMC.
- We find low $[\text{Ba}/\text{Eu}]$ and $[\text{La}/\text{Eu}]$ for the old clusters in our sample, which indicates that r -process products dominated the neutron-capture chemical enrichment at early times in the LMC.
- We find high $[\text{Ba}/\text{Eu}]$ and $[\text{La}/\text{Eu}]$ in the younger clusters in our sample, which indicates that there was significant enrichment with s -process products at later times in the LMC.
- We obtain consistently high $[\text{Eu}/\text{Ca}]$ for all of the clusters in our sample.

As a whole, our results are consistent with low efficiency or prolonged star formation between the bursts of star formation in which these massive clusters formed (e.g. Harris & Zaritsky 2009; Carrera et al. 2008; Bica et al. 1986; Olszewski et al. 1991). The early, rapid

burst of star formation in the LMC is reflected in high $[\alpha/\text{Fe}]$ and high r -process heavy element composition. The period of prolonged, or inefficient star formation is reflected in the steady increase in the s -process fraction toward high metallicities and younger ages, and perhaps in our observations of low $[\text{Mn}/\text{Fe}]$ and $[\text{Cu}/\text{Fe}]$ at high metallicity.

Several general scenarios could produce such a star formation and chemical evolution history. One possibility is a “leaky-box” scenario in which enriched gas from a first generation of star formation and SNe II is lost in outflows. However that is difficult to quantitatively distinguish from a situation in which there is a combination of both outflows and inflows of low-metallicity gas (see modeling of the LMC age- $[\text{Fe}/\text{H}]$ relationship by Carrera et al. (2008)). Clearly there is current evidence for both ongoing accretion and gas stripping in the LMC (e.g. see Besla et al. (2010); Nidever et al. (2010); Olsen et al. (2011)). Finally, the analytical dual-burst chemical evolution model of Pagel & Tautvaišienė (1998) describes the well known age-metallicity relationship for the LMC very well. However, this new data with fine age and $[\text{Fe}/\text{H}]$ resolution reveals that the simple model does not describe the chemical evolution of other elements as well. Our data set provides new constraints for future, more sophisticated, models of the star formation history of the LMC.

This research was supported by NSF grant AST-0507350. J.E.C. thanks N. Calvet, P. GuhaThakurta, M. Mateo, M. S. Oey, and G. Evrard for careful reading of an early version of the manuscript. The authors thank

D. Osip for help with the scanning algorithm for MIKE on the Magellan Clay Telescope.

REFERENCES

- Arlandini, C., Käppeler, F., Wisshak, K., Gallino, R., Lugaro, M., Busso, M., & Straniero, O. 1999, *ApJ*, 525, 886
- Asplund, M., Grevesse, N., & Sauval, A. J. 2005, in *Astronomical Society of the Pacific Conference Series*, Vol. 336, *Cosmic Abundances as Records of Stellar Evolution and Nucleosynthesis*, ed. T. G. Barnes, III & F. N. Bash, 25–+
- Baumgardt, H., & Makino, J. 2003, *MNRAS*, 340, 227
- Bensby, T., Feltzing, S., Lundström, I., & Ilyin, I. 2005, *A&A*, 433, 185
- Bernstein, R., Shtetman, S. A., Gunnels, S. M., Mochnacki, S., & Athey, A. E. 2003, in *Society of Photo-Optical Instrumentation Engineers (SPIE) Conference Series*, Vol. 4841, *Society of Photo-Optical Instrumentation Engineers (SPIE) Conference Series*, ed. M. Iye & A. F. M. Moorwood, 1694–1704
- Besla, G., Kallivayalil, N., Hernquist, L., van der Marel, R. P., Cox, T. J., & Kereš, D. 2010, *ApJ*, 721, L97
- Bica, E., Dottori, H., & Pastoriza, M. 1986, *A&A*, 156, 261
- Bisterzo, S., Pompeia, L., Gallino, R., Pignatari, M., Cunha, K., Heger, A., & Smith, V. 2005, *Nuclear Physics A*, 758, 284
- Brodie, J. P., & Strader, J. 2006, *ARA&A*, 44, 193
- Busso, M., Gallino, R., & Wasserburg, G. J. 1999, *ARA&A*, 37, 239
- Cameron, S. A. 2009, PhD thesis, University of Michigan (Paper II)
- Carrera, R., Gallart, C., Hardy, E., Aparicio, A., & Zinn, R. 2008, *AJ*, 135, 836
- Carretta, E. 2006, *AJ*, 131, 1766
- Carretta, E., Bragaglia, A., Gratton, R. G., Recio-Blanco, A., Lucatello, S., D’Orazi, V., & Cassisi, S. 2010, *A&A*, 516, A55+
- Cescutti, G., Matteucci, F., Lanfranchi, G. A., & McWilliam, A. 2008, *A&A*, 491, 401
- Cioni, M., Girardi, L., Marigo, P., & Habing, H. J. 2006, *A&A*, 448, 77
- Cole, A. A., Smecker-Hane, T. A., & Gallagher, III, J. S. 2000, *AJ*, 120, 1808
- Colucci, J. E., & Bernstein, R. A. 2011, submitted (CB11)
- Colucci, J. E., Bernstein, R. A., Cameron, S., McWilliam, A., & Cohen, J. G. 2009, *ApJ*, 704, 385
- Colucci, J. E., Bernstein, R. A., Cameron, S. A., & McWilliam, A. 2011, *ApJ*, 735, 55 (Paper III)
- Conroy, C. 2011, *ArXiv e-prints*
- Conroy, C., & Spergel, D. N. 2011, *ApJ*, 726, 36
- D’Antona, F., & Ventura, P. 2007, *MNRAS*, 379, 1431
- de Mink, S. E., Pols, O. R., Langer, N., & Izzard, R. G. 2009, *A&A*, 507, L1
- Decressin, T., Meynet, G., Charbonnel, C., Prantzos, N., & Ekström, S. 2007, *A&A*, 464, 1029
- D’Ercole, A., Vesperini, E., D’Antona, F., McMillan, S. L. W., & Recchi, S. 2008, *MNRAS*, 391, 825
- Drukier, G. A. 1995, *ApJS*, 100, 347
- Ferraro, F. R., Mucciarelli, A., Carretta, E., & Origlia, L. 2006, *ApJ*, 645, L33
- Geha, M. C., et al. 1998, *AJ*, 115, 1045
- Geisler, D., Wallerstein, G., Smith, V. V., & Casetti-Dinescu, D. I. 2007, *PASP*, 119, 939
- Goudfrooij, P., Puzia, T. H., Kozhurina-Platais, V., & Chandar, R. 2011, *ApJ*, 737, 3
- Gratton, R., Sneden, C., & Carretta, E. 2004, *ARA&A*, 42, 385
- Gratton, R. G., Carretta, E., Eriksson, K., & Gustafsson, B. 1999, *A&A*, 350, 955
- Grevesse, N. 1989, *Cosmic Abundances of Matter*, 183, 9
- Harris, J., & Zaritsky, D. 2009, *AJ*, 138, 1243
- Hill, V., Andrievsky, S., & Spite, M. 1995, *A&A*, 293, 347 (H95)
- Hill, V., François, P., Spite, M., Primas, F., & Spite, F. 2000, *A&A*, 364, L19 (H00)
- Jasniewicz, G., & Thevenin, F. 1994, *A&A*, 282, 717
- Johnson, J. A., Ivans, I. I., & Stetson, P. B. 2006, *ApJ*, 640, 801 (J06)
- Kurucz, R. L. 1997, in *IAU Symposium*, Vol. 189, *IAU Symposium*, ed. T. R. Bedding, A. J. Booth, & J. Davis, 217–226
- Leitherer, C. 2001, in *Astronomical Society of the Pacific Conference Series*, Vol. 245, *Astrophysical Ages and Times Scales*, ed. T. von Hippel, C. Simpson, & N. Manset, 390–+
- Luck, R. E., & Lambert, D. L. 1992, *ApJS*, 79, 303 (LL92)
- Mackey, A. D., Broby Nielsen, P., Ferguson, A. M. N., & Richardson, J. C. 2008, *ApJ*, 681, L17
- Marín-Franch, A., et al. 2009, *ApJ*, 694, 1498
- Matteucci, F., Raiteri, C. M., Busson, M., Gallino, R., & Gratton, R. 1993, *A&A*, 272, 421
- McLaughlin, D. E., & van der Marel, R. P. 2005, *ApJS*, 161, 304
- McWilliam, A. 1998, *AJ*, 115, 1640
- McWilliam, A., & Bernstein, R. A. 2008, *ApJ*, 684, 326 (Paper I)
- McWilliam, A., Preston, G. W., Sneden, C., & Searle, L. 1995a, *AJ*, 109, 2757
- McWilliam, A., Preston, G. W., Sneden, C., & Shtetman, S. 1995b, *AJ*, 109, 2736
- McWilliam, A., & Rich, R. M. 1994, *ApJS*, 91, 749
- McWilliam, A., Rich, R. M., & Smecker-Hane, T. A. 2003, *ApJ*, 592, L21
- McWilliam, A., & Smecker-Hane, T. A. 2005, *ApJ*, 622, L29
- Meléndez, J., & Barbuy, B. 2009, *A&A*, 497, 611
- Meylan, G., Dubath, P., & Mayor, M. 1991, in *Astronomical Society of the Pacific Conference Series*, Vol. 13, *The Formation and Evolution of Star Clusters*, ed. K. Janes, 158–160
- Milone, A. P., Bedin, L. R., Piotto, G., & Anderson, J. 2009, *A&A*, 497, 755
- Mucciarelli, A., Carretta, E., Origlia, L., & Ferraro, F. R. 2008, *AJ*, 136, 375 (M08)
- Mucciarelli, A., et al. 2011, *MNRAS*, 413, 837 (M11)
- Mucciarelli, A., Origlia, L., & Ferraro, F. R. 2010, *ApJ*, 717, 277 (M10)
- Mucciarelli, A., Origlia, L., Ferraro, F. R., & Pancino, E. 2009, *ApJ*, 695, L134
- Nidever, D. L., Majewski, S. R., Butler Burton, W., & Nigra, L. 2010, *ApJ*, 723, 1618
- Olsen, K. A. G., Zaritsky, D., Blum, R. D., Boyer, M. L., & Gordon, K. D. 2011, *ArXiv e-prints*
- Olszewski, E. W., Schommer, R. A., Suntzeff, N. B., & Harris, H. C. 1991, *AJ*, 101, 515
- Olszewski, E. W., Suntzeff, N. B., & Mateo, M. 1996, *ARA&A*, 34, 511
- Pagel, B. E. J., & Tautvaisiene, G. 1998, *MNRAS*, 299, 535
- Piotto, G., et al. 2007, *ApJ*, 661, L53
- Pompéia, L., et al. 2008, *A&A*, 480, 379 (P08)
- Pritzl, B. J., Venn, K. A., & Irwin, M. 2005, *AJ*, 130, 2140
- Russell, S. C., & Bessell, M. S. 1989, *ApJS*, 70, 865 (RB89)
- Sbordone, L., Bonifacio, P., Buonanno, R., Marconi, G., Monaco, L., & Zaggia, S. 2007, *A&A*, 465, 815
- Shetrone, M., Venn, K. A., Tolstoy, E., Primas, F., Hill, V., & Kaufer, A. 2003, *AJ*, 125, 684
- Shetrone, M. D., Côté, P., & Sargent, W. L. W. 2001, *ApJ*, 548, 592
- Simmerer, J., Sneden, C., Cowan, J. J., Collier, J., Woolf, V. M., & Lawler, J. E. 2004, *ApJ*, 617, 1091
- Smecker-Hane, T. A., & McWilliam, A. 2002, *ArXiv Astrophysics e-prints*
- Smith, V. V., et al. 2002, *AJ*, 124, 3241
- Sneden, C., Cowan, J. J., & Gallino, R. 2008, *ARA&A*, 46, 241
- Sneden, C. A. 1973, PhD thesis, THE UNIVERSITY OF TEXAS AT AUSTIN.
- Spite, F., Barbuy, B., & Spite, M. 1993, *A&A*, 272, 116
- Tinsley, B. M. 1979, *ApJ*, 229, 1046
- Tolstoy, E., Hill, V., & Tosi, M. 2009, *ARA&A*, 47, 371
- Venn, K. A., Irwin, M., Shetrone, M. D., Tout, C. A., Hill, V., & Tolstoy, E. 2004, *AJ*, 128, 1177
- Woolsey, S. E., & Weaver, T. A. 1995, *ApJS*, 101, 181

Table 1
LMC Cluster Properties

Cluster	Age ^a ILS	[Fe/H] ILS	[α /Fe] ^b Lit	Ref. ^c
Old (> 5 Gyrs)				
NGC 1916	>5	-1.54 ± 0.04	...	
NGC 2019	>7	-1.67 ± 0.03	+0.20	1
NGC 2005	>5	-1.54 ± 0.04	+0.05	1
Intermediate Age (1-3 Gyrs)				
NGC 1978	1.0-3.0	-0.54 ± 0.18	+0.02, +0.38	2, 3
NGC 1718	1.0-2.5	-0.70 ± 0.03	...	
Young (< 1 Gyr)				
NGC 1866	0.10-0.50	-0.27 ± 0.16	+0.08,+0.00	3,4
NGC 1711	0.06-0.10	-0.57 ± 0.07	...	
NGC 2100	<0.04	$-0.40 <[\text{Fe}/\text{H}] < +0.03$	-0.06	5

^a Ages listed in Gyrs

^b Mean of [Si/Fe], [Ca/Fe], and [Ti/Fe] abundances from 1, 2, 4 and 5, and mean of [O/Fe] from 3.

^c References for column 5: 1. J06, 2. M08, 3. H00, 4. M11, 5. Jasniewicz & Thevenin (1994)

Table 2
Line Parameters and Integrated Light Equivalent Widths for LMC GCs

Species	λ (Å)	E.P. (eV)	$\log gf$	EW(mÅ)	EW(mÅ)	EW(mÅ)	EW(mÅ)	EW(mÅ)	EW(mÅ)	EW(mÅ)	type	
				1916	2005	2019	1978	1718	1866	1711		2100
O I	7771.941	9.146	0.369	0.00	0.00	0.00	113.7	SYN
O I	7775.391	9.146	0.001	92.0	SYN
Na I	5682.650	2.100	-0.700	27.7	56.7	39.9	121.2	66.5	73.6	SYN
Na I	5688.220	2.100	-0.460	78.2	61.0	55.4	114.6	92.6	87.1	SYN
Na I	6154.230	2.100	-1.570	47.6	SYN
Na I	6160.753	2.100	-1.270	25.8	74.8	45.9	35.6	SYN
Mg I	4571.102	0.000	-5.569	52.5	EW
Mg I	4703.003	4.346	-0.377	106.4	...	82.0	113.7	EW
Mg I	4703.003	4.346	-0.377	150.7	EW
Mg I	5528.418	4.346	-0.341	149.6	121.9	115.9	175.4	99.9	118.6	SYN
Mg I	5711.090	4.340	-1.630	46.5	EW
Al I	6696.032	3.140	-1.481	29.9	...	25.0	...	29.5	28.5	...	53.5	SYN
Al I	6698.669	3.140	-1.782	33.3	SYN
Si I	5684.500	4.950	-1.650	83.4	SYN
Si I	7405.790	5.610	-0.660	50.4	...	31.5	66.7	...	86.5	SYN
Si I	7415.958	5.610	-0.730	16.3	89.5	...	82.9	SYN
Ca I	4454.793	1.899	0.260	128.6	EW
Ca I	5349.469	2.709	-0.310	33.5	EW
Ca I	5581.979	2.523	-0.555	47.0	EW
Ca I	5588.764	2.526	0.358	72.5	129.0	84.7	113.4	EW
Ca I	5590.126	2.521	-0.571	39.4	89.5	...	63.1	...	68.2	EW
Ca I	5601.286	2.526	-0.690	48.7	53.5	56.5	EW
Ca I	5857.459	2.933	0.240	...	57.5	91.2	34.7	102.3	EW
Ca I	5867.572	2.930	-0.801	41.7	EW
Ca I	6102.727	1.879	-0.790	...	69.2	93.7	EW
Ca I	6102.727	1.879	-0.790	86.7	EW
Ca I	6122.226	1.886	-0.320	149.5	...	102.9	135.8	...	131.0	EW
Ca I	6122.226	1.886	-0.320	101.5	EW
Ca I	6162.180	1.899	-0.090	136.1	...	150.7	134.0	96.3	...	EW
Ca I	6166.440	2.520	-1.142	26.8	94.6	EW
Ca I	6169.044	2.520	-0.797	69.7	EW
Ca I	6169.564	2.526	-0.478	144.0	25.0	89.4	EW
Ca I	6439.083	2.526	0.390	127.4	115.7	104.2	...	151.3	123.2	...	138.5	EW
Ca I	6455.605	2.523	-1.290	95.9	71.4	EW
Ca I	6462.680	2.523	0.262	...	102.5	74.0	EW
Ca I	6471.668	2.526	-0.686	62.3	69.1	97.9	EW
Ca I	6493.788	2.521	-0.109	...	99.5	76.1	EW
Ca I	6493.788	2.521	-0.109	74.0	EW
Ca I	6572.795	0.000	-4.310	57.7	EW
Ca I	7148.150	2.709	0.137	90.5	...	96.8	111.5	...	143.6	EW
Sc II	4246.837	0.315	0.240	106.1	EW/HFS
Sc II	4314.091	0.618	-0.100	76.3	EW/HFS
Sc II	4670.413	1.357	-0.580	22.0	EW/HFS
Sc II	5526.821	1.768	0.020	59.1	62.8	48.6	59.0	66.6	78.2	EW/HFS
Sc II	5667.150	1.500	-1.360	27.5	83.2	EW/HFS
Sc II	6245.620	1.510	-1.070	62.5	EW/HFS
Sc II	6604.600	1.357	-1.480	23.3	88.6	EW/HFS
Ti I	4533.249	0.848	0.476	71.5	EW
Ti I	4534.785	0.836	0.280	51.0	EW
Ti I	4981.740	0.848	0.504	...	135.2	62.8	EW
Ti I	4991.072	0.836	0.380	69.5	EW
Ti I	4999.510	0.826	0.250	69.9	...	122.3	EW
Ti I	5014.240	0.813	0.110	...	74.0	66.8	EW
Ti I	5039.964	0.021	-1.130	46.8	...	94.4	77.2	EW
Ti I	5064.658	0.048	-0.991	77.3	EW
Ti I	5173.749	0.000	-1.118	85.4	...	51.1	EW
Ti I	5192.978	0.021	-1.006	90.2	EW
Ti I	5210.392	0.048	-0.884	84.1	...	73.0	EW
Ti I	5866.461	1.067	-0.840	37.6	96.4	EW
Ti I	6064.600	1.050	-1.890	20.9	64.2	EW
Ti I	6126.200	1.070	-1.370	25.9	...	59.6	43.8	...	73.0	EW
Ti I	6554.238	1.443	-1.218	33.2	71.6	EW
Ti I	6743.127	0.900	-1.630	65.3	102.4	EW
Ti II	4394.068	1.221	-1.590	58.6	EW
Ti II	4395.040	1.084	-0.660	...	131.2	EW
Ti II	4395.848	1.243	-2.170	51.9	EW

Table 2 — *Continued*

Species	λ (Å)	E.P. (eV)	$\log gf$	EW(mÅ) 1916	EW(mÅ) 2005	EW(mÅ) 2019	EW(mÅ) 1978	EW(mÅ) 1718	EW(mÅ) 1866	EW(mÅ) 1711	EW(mÅ) 2100	type
Ti II	4399.778	1.237	-1.270	78.5	EW
Ti II	4418.342	1.237	-2.460	...	65.7	EW
Ti II	4468.500	1.130	-0.600	92.2	EW
Ti II	4501.278	1.116	-0.750	81.2	EW
Ti II	4563.766	1.221	-0.960	110.4	72.6	61.0	EW
Ti II	4571.982	1.572	-0.530	137.8	130.9	81.1	EW
Ti II	4589.953	1.237	-1.790	102.0	66.6	64.6	EW
Ti II	5129.162	1.892	-1.390	102.0	104.4	EW
Ti II	5185.908	1.893	-1.350	92.6	EW
Ti II	5188.698	1.582	-1.210	118.2	90.5	64.3	EW
Ti II	5336.794	1.582	-1.700	57.2	42.5	39.1	EW
Ti II	5381.010	1.566	-2.080	...	68.8	47.1	EW
V I	6090.210	1.080	-0.060	25.6	101.3	42.0	46.0	EW/HFS
V I	6090.210	1.080	-0.060	27.1	EW/HFS
V I	6111.590	1.040	-0.720	31.5	EW/HFS
V I	6119.500	1.060	-0.320	42.94	EW/HFS
V I	6135.350	1.050	-0.750	70.5	EW/HFS
V I	6199.140	0.290	-1.300	84.6	EW/HFS
V I	6216.430	0.280	-0.810	37.1	EW/HFS
V I	6233.170	0.280	-2.070	19.9	EW/HFS
V I	6531.429	1.220	-0.840	43.5	50.7	EW/HFS
Cr I	5204.470	0.940	-0.210	153.3	EW
Cr I	5206.044	0.941	0.019	127.8	EW
Cr I	5208.432	0.941	0.158	146.3	...	164.2	EW
Cr I	5296.700	0.980	-1.400	57.7	EW
Cr I	5345.807	1.004	-0.980	72.3	64.8	69.3	90.4	EW
Cr I	5348.340	1.000	-1.290	66.8	74.4	61.0	EW
Cr I	5409.799	1.030	-0.720	111.3	85.0	102.9	...	125.9	136.6	EW
Cr I	5787.930	3.320	-0.080	59.0	EW
Cr I	6330.096	0.941	-2.920	21.0	...	68.2	EW
Cr I	7400.188	2.900	-0.111	34.9	EW
Cr I	7462.342	2.914	-0.010	60.7	EW
Mn I	4033.072	0.000	-0.618	73.9	...	EW/HFS
Mn I	5394.670	0.000	-3.500	59.6	56.4	40.2	118.3	EW/HFS
Mn I	5420.270	2.140	-1.460	43.1	25.8	37.5	84.8	72.6	...	28.8	...	EW/HFS
Mn I	5432.530	0.000	-3.800	51.7	...	41.5	118.5	68.7	EW/HFS
Mn I	5516.670	2.180	-1.850	94.0	EW/HFS
Mn I	6013.500	3.070	-0.250	36.9	...	31.5	85.0	64.9	...	36.2	60.5	EW/HFS
Mn I	6016.640	3.070	-0.216	41.0	...	40.5	88.0	79.8	...	35.3	65.1	EW/HFS
Mn I	6021.800	3.070	0.034	41.8	...	47.1	93.0	59.5	...	35.8	51.1	EW/HFS
Co I	5483.350	1.710	-1.410	34.8	EW/HFS
Co I	6814.961	1.956	-1.900	EW/HFS
Co I	7052.870	1.956	-1.620	22.7	EW/HFS
Ni I	5084.100	3.680	0.030	39.2	49.7	EW
Ni I	5435.880	1.990	-2.590	16.5	EW
Ni I	6108.100	1.680	-2.450	33.9	89.5	50.1	50.5	...	91.8	EW
Ni I	6108.100	1.680	-2.450	39.9	...	50.1	50.5	...	91.8	EW
Ni I	6128.900	1.680	-3.330	68.4	EW
Ni I	6314.650	1.940	-1.770	33.4	EW
Ni I	6327.604	1.676	-3.150	33.5	98.6	21.3	...	49.7	31.9	...	59.1	EW
Ni I	6339.118	4.150	-0.550	49.1	EW
Ni I	6482.809	1.935	-2.630	28.3	74.0	EW
Ni I	6586.319	1.951	-2.810	39.2	32.8	...	EW
Ni I	6643.638	1.676	-2.300	63.0	53.1	58.9	...	87.2	74.9	50.8	99.8	EW
Ni I	6767.784	1.826	-2.170	51.2	51.2	61.6	55.2	52.7	84.2	EW
Ni I	6772.321	3.660	-0.980	57.5	EW
Ni I	7110.905	1.935	-2.980	24.0	EW
Ni I	7122.206	3.542	0.040	61.2	...	71.0	70.7	...	108.6	EW
Ni I	7393.609	3.606	-0.270	44.1	...	51.8	54.6	...	EW
Ni I	7414.514	1.986	-2.570	46.1	EW
Ni I	7422.286	3.635	-0.140	55.3	EW
Ni I	7522.778	3.660	-0.400	56.3	EW
Ni I	7525.118	3.635	-0.520	41.8	52.7	EW
Ni I	7555.607	3.850	0.110	68.2	...	42.3	74.9	...	105.0	EW
Cu I	5782.050	1.640	-2.920	121.0	SYN/HFS
Sr II	4215.539	0.000	-0.170	112.9	...	126.5	SYN/HFS
Y II	4883.685	1.084	0.070	46.0	...	27.9	103.8	59.6	54.6	...	49.0	SYN

Table 2 — *Continued*

Species	λ (Å)	E.P. (eV)	$\log gf$	EW(mÅ) 1916	EW(mÅ) 2005	EW(mÅ) 2019	EW(mÅ) 1978	EW(mÅ) 1718	EW(mÅ) 1866	EW(mÅ) 1711	EW(mÅ) 2100	type
Y II	5087.420	1.080	-0.170	78.2	EW
Ba II	4554.036	0.000	0.163	118.7	...	127.4	EW/HFS
Ba II	4934.095	0.000	-0.157	51.4	...	51.3	EW/HFS
Ba II	5853.688	0.604	-1.010	54.3	...	48.4	130.0	60.4	118.4	...	57.8	SYN/HFS
Ba II	6141.727	0.704	-0.077	131.4	108.8	101.2	119.6	66.7	116.4	SYN/HFS
Ba II	6496.908	0.604	-0.377	113.5	...	106.0	...	177.6	...	68.9	107.2	SYN/HFS
La II	5114.510	0.240	-1.030	44.2	SYN/HFS
La II	6390.480	0.321	-1.520	23.3	71.0	...	52.9	SYN/HFS
Nd II	5249.590	0.976	0.217	27.1	...	27.9	58.4	...	40.7	SYN
Nd II	5319.820	0.550	-0.194	48.9	58.8	SYN
Sm II	4537.954	0.485	-0.230	33.1	45.3	...	45.2	SYN
Eu II	6645.127	1.380	0.204	22.4	...	22.4	48.1	22.8	55.5	SYN/HFS

Note. — Lines listed twice correspond to those measured in adjacent orders with overlapping wavelength coverage. Abundances that are calculated using EWs are labeled “EW” in Column 13, and abundances that are calculated using line synthesis are labeled “SYN.” Abundances that were calculated with hyperfine splitting of energy levels are noted as “HFS” in Column 13. $\log gf$ values are taken from Paper I, Paper II, Colucci et al. (2009), Meléndez & Barbuy (2009) and references therein, as well as the Kurucz atomic and molecular line database (Kurucz 1997). Hfs line lists and A and B constants were taken from McWilliam & Rich (1994), McWilliam et al. (1995a), McWilliam et al. (1995b), McWilliam (1998), J06 and (Kurucz 1997).

Table 3
Line Parameters and Stellar Equivalent Widths

Species	λ (Å)	E.P. (eV)	$\log gf$	EW (mÅ) 1978 737	EW (mÅ) 1978 730	EW (mÅ) 1866 954	EW (mÅ) 1866 1653	EW (mÅ) 1667	EW (mÅ) 831	EW (mÅ) 988	EW (mÅ) 1194	EW (mÅ) 1711 2100 c12	EW (mÅ) 2100 b22	Note
O I	6300.311	0.000	-9.750	SYN	SYN	SYN	SYN	SYN	SYN	SYN	SYN	...	SYN	
Na I	5682.650	2.100	-0.700	SYN	SYN	SYN	SYN	SYN	SYN	SYN	
Na I	5688.220	2.100	-0.460	...	SYN	SYN	SYN	SYN	SYN	SYN	
Na I	6154.230	2.100	-1.570	SYN	SYN	SYN	SYN	SYN	SYN	SYN	SYN	SYN	SYN	
Na I	6160.753	2.100	-1.270	SYN	SYN	SYN	SYN	SYN	SYN	SYN	SYN	SYN	SYN	
Mg I	5711.090	4.340	-1.630	...	136.6	...	163.3	129.5	163.8	68.4	...	89.6	198.5	
Mg I	6319.242	5.110	-2.210	72.3	47.6	78.9	59.0	64.6	51.9	19.7	52.1	
Mg I	6965.408	5.750	-1.720	44.2	...	42.3	22.3	39.9	
Mg I	7387.700	5.750	-0.870	71.5	74.9	69.1	61.5	39.8	58.9	87.8	75.6	
Mg I	8473.690	5.930	-2.020	56.8	28.5	33.2	23.5	
Mg I	8473.690	5.930	-2.020	21.9	
Mg I	8923.570	5.390	-1.570	99.5	
Al I	6696.032	3.140	-1.480	SYN	SYN	SYN	...	SYN	SYN	SYN	SYN	SYN	SYN	
Al I	6698.669	3.140	-1.780	SYN	SYN	SYN	...	SYN	SYN	SYN	...	SYN	SYN	
Al I	7835.310	4.020	-0.650	SYN	SYN	SYN	SYN	
Si I	5684.500	4.950	-1.650	39.3	28.3	79.9	...	150.0	59.3	47.9	60.2	
Si I	5690.400	4.930	-1.870	...	61.2	66.1	...	57.6	48.8	31.1	53.2	88.1	73.0	
Si I	5793.080	4.930	-2.060	36.6	43.0	...	SYN	56.5	47.6	45.8	48.1	58.0	53.0	
Si I	5948.500	5.080	-1.230	83.3	63.9	104.1	SYN	...	74.5	71.1	73.6	...	99.8	
Si I	6237.328	5.610	-1.010	52.6	100.4	68.4	46.2	41.6	
Si I	6721.844	5.860	-1.170	46.5	96.7	61.5	43.4	29.4	40.7	
Si I	6976.504	5.950	-1.040	36.7	33.3	36.4	
Si I	7235.325	5.610	-1.460	46.9	33.0	32.4	25.9	32.1	...	
Si I	7405.790	5.610	-0.660	54.2	52.0	95.0	75.5	79.8	...	118.8	118.2	
Si I	7415.363	5.620	-1.700	...	37.6	66.6	46.1	17.0	
Si I	7415.958	5.610	-0.730	62.1	62.4	120.0	72.6	117.0	118.8	
Si I	7423.509	5.620	-0.580	...	68.0	80.9	96.5	
Si I	7932.350	5.960	-0.470	...	46.9	71.4	
Ca I	5260.400	2.520	-1.720	93.9	104.3	135.9	117.6	
Ca I	5581.979	2.520	-0.560	...	163.1	144.8	184.4	164.2	179.8	94.0	
Ca I	5590.126	2.520	-0.570	...	158.8	155.2	156.5	125.1	173.9	84.7	
Ca I	5590.126	2.520	-0.570	...	149.8	
Ca I	5601.286	2.530	-0.690	97.3	
Ca I	5601.286	2.530	-0.690	98.9	
Ca I	5867.572	2.930	-0.800	...	95.2	63.1	...	90.1	

Table 3 — *Continued*

Species	λ (Å)	E.P. (eV)	log gf	EW	EW	EW	EW	EW	EW	EW	EW	EW	EW	Note
				(mÅ) 1978 737	(mÅ) 1978 730	(mÅ) 1866 954	(mÅ) 1866 1653	(mÅ) 1866 1667	(mÅ) 1711 831	(mÅ) 1711 988	(mÅ) 1711 1194	(mÅ) 2100 c12	(mÅ) 2100 b22	
Ca I	5867.572	2.930	-0.800	...	67.4	
Ca I	6156.020	2.520	-2.500	60.7	85.0	39.8	15.4	76.3
Ca I	6166.440	2.520	-1.140	167.2	...	132.6	172.8	117.0	153.5	47.8	167.8
Ca I	6169.044	2.520	-0.800	176.6	142.8	150.0	163.1	150.0	185.6	82.6	
Ca I	6169.044	2.520	-0.800	166.4	...	146.3	76.2	
Ca I	6169.564	2.530	-0.480	165.9	...	167.7	...	98.1	
Ca I	6417.685	4.440	-2.300	...	75.3	
Ca I	6449.820	2.520	-0.500	101.2	
Ca I	6455.605	2.520	-1.290	130.4	126.7	117.3	...	114.2	133.7	37.3	155.4	172.8
Ca I	6464.679	2.530	-4.270	...	107.2	
Ca I	6471.668	2.530	-0.690	165.6	166.5	137.9	177.8	84.4	
Ca I	6493.788	2.520	-0.110	175.5	...	25.5	
Ca I	6508.846	2.530	-2.160	89.2	104.1	56.8	...	63.1	103.3
Ca I	6572.795	0.000	-4.310	13.4	
Ca I	6719.687	2.710	-2.550	13.3	...	15.6	
Sc I	6210.671	0.000	-1.570	172.2	...	96.6	126.7	74.4	160.7	7.0	HFS
Sc II	5031.024	1.360	-0.400	143.5	13.9	
Sc II	5526.821	1.770	0.020	...	117.2	124.8	150.2	131.9	148.9	86.0	141.0	...	189.7	HFS
Sc II	5640.990	1.500	-1.130	115.9	116.2	112.6	141.8	113.8	117.8	135.2	121.6	175.7	171.0	HFS
Sc II	5657.880	1.510	-0.600	119.0	110.7	131.9	152.5	122.8	136.6	121.2	HFS
Sc II	5667.150	1.500	-1.360	95.0	84.8	112.0	141.6	116.1	81.9	111.7	82.7	HFS
Sc II	6245.620	1.510	-1.070	86.0	78.2	98.2	110.1	94.0	87.1	118.5	HFS
Sc II	6604.600	1.360	-1.480	99.3	96.2	99.8	122.5	97.7	89.3	99.7	...	163.8	...	HFS
Ti I	4981.740	0.850	0.500	96.6	
Ti I	5039.964	0.020	-1.130	79.9	
Ti I	5064.658	0.050	-0.990	78.3	
Ti I	5064.658	0.050	-0.990	64.3	
Ti I	5173.749	0.000	-1.120	81.5	
Ti I	5173.749	0.000	-1.120	79.0	
Ti I	5192.978	0.020	-1.010	96.2	
Ti I	5210.392	0.050	-0.880	80.2	
Ti I	5210.392	0.050	-0.880	80.3	
Ti I	5223.630	2.090	-0.560	101.9	104.5	...	139.1	64.0	...	38.7	129.9	
Ti I	5223.630	2.090	-0.560	133.3	61.64	
Ti I	5295.780	1.070	-1.580	127.8	...	90.3	...	98.1	...	89.6	
Ti I	5338.330	0.830	-1.870	...	134.1	76.4	131.4	46.9	...	8.4	...	158.8	...	
Ti I	5384.630	0.830	-2.910	118.1	127.2	...	134.3	...	74.9	80.9	142.0	
Ti I	5401.320	0.820	-2.890	...	134.0	...	128.0	76.4	107.8	180.3	176.7	
Ti I	5401.320	0.820	-2.890	...	142.0	...	148.1	182.6	...	
Ti I	5453.650	1.440	-1.610	129.8	103.5	82.5	94.3	
Ti I	5471.205	1.440	-1.400	119.5	160.4	67.4	136.3	71.3	116.2	...	127.2	178.4	194.1	
Ti I	5474.230	1.460	-1.230	152.0	...	158.3	
Ti I	5474.230	1.460	-1.230	148.5	
Ti I	5503.900	2.580	0.020	101.2	119.5	...	126.4	79.6	80.3	6.9	79.7	167.7	161.5	
Ti I	5648.570	2.500	-0.260	95.7	95.6	...	119.2	78.5	76.1	...	77.3	116.2	122.2	
Ti I	5866.461	1.070	-0.840	154.0	...	24.0	
Ti I	5866.461	1.070	-0.840	147.3	...	25.5	
Ti I	6064.600	1.050	-1.890	153.0	168.5	101.6	154.4	
Ti I	6064.600	1.050	-1.890	141.0	158.4	100.2	155.2	
Ti I	6126.200	1.070	-1.370	142.6	185.2	131.1	...	14.9	
Ti I	6303.767	1.440	-1.570	132.6	144.2	112.8	136.6	...	132.3	...	138.1	...	180.7	
Ti I	6303.767	1.440	-1.570	139.3	138.2	113.9	166.1	...	118.0	
Ti I	6554.238	1.440	-1.220	168.3	101.1	122.4	164.6	107.9	142.5	15.1	219.2	
Ti I	6556.077	1.460	-1.070	148.1	170.2	...	162.7	11.3	
Ti I	6556.077	1.460	-1.070	136.0	178.2	
Ti I	6559.576	2.050	-2.130	70.6	68.0	76.6	65.4	
Ti I	6743.127	0.900	-1.630	141.9	...	134.5	178.3	8.6	
Ti I	7138.930	1.440	-1.590	178.4	...	101.8	164.0	86.6	102.4	...	107.7	
Ti I	7209.468	1.460	-0.500	153.5	...	21.3	
Ti I	7216.190	1.440	-1.150	163.6	170.5	155.3	82.1	70.2	
Ti I	7251.717	1.430	-0.770	22.5	
Ti II	4589.953	1.240	-1.790	143.5	
Ti II	4589.953	1.240	-1.790	148.8	
Ti II	4865.618	1.120	-2.610	...	117.1	122.4	107.1	46.3	...	179.1	186.8	
Ti II	5185.908	1.890	-1.350	141.3	19.8	198.0	
Ti II	5336.794	1.580	-1.700	161.1	
Ti II	7214.741	2.590	-1.740	65.4	101.0	69.5	78.0	74.4	
V I	4851.470	0.000	-1.140	164.7	HFS

Table 3 — *Continued*

Species	λ (Å)	E.P. (eV)	log gf	EW	EW	EW	EW	EW	EW	EW	EW	EW	EW	Note
				(mÅ) 1978 737	(mÅ) 1978 730	(mÅ) 1866 954	(mÅ) 1866 1653	(mÅ) 1866 1667	(mÅ) 1711 831	(mÅ) 1711 988	(mÅ) 1711 1194	(mÅ) 2100 c12	(mÅ) 2100 b22	
V I	6039.730	1.060	-0.650	136.9	149.8	96.8	138.9	...	139.8	...	157.7	HFS
V I	6081.400	1.050	-0.580	168.0	175.1	128.7	182.4	HFS
V I	6081.400	1.050	-0.580	164.0	...	123.8	HFS
V I	6090.210	1.080	-0.060	131.7	188.2	16.4	HFS
V I	6090.210	1.080	-0.060	134.5	12.2	HFS
V I	6111.590	1.040	-0.720	117.6	...	123.4	...	12.2	HFS
V I	6119.500	1.060	-0.320	164.2	...	125.4	...	66.3	...	8.2	HFS
V I	6135.350	1.050	-0.750	158.0	174.8	110.6	...	105.3	...	5.2	HFS
V I	6199.140	0.290	-1.300	165.1	...	155.0	...	14.3	HFS
V I	6199.140	0.290	-1.300	165.2	HFS
V I	6216.430	0.280	-0.810	168.6	...	163.6	...	14.0	HFS
V I	6224.470	0.290	-2.010	112.0	179.0	97.4	HFS
V I	6233.170	0.280	-2.070	95.1	...	84.9	184.5	HFS
V I	6251.760	0.290	-1.340	142.4	HFS
V I	6274.658	0.270	-1.670	...	174.1	136.0	...	141.5	...	13.1	HFS
V I	6504.186	1.180	-1.230	116.6	129.5	70.6	...	71.7	81.8	...	87.2	...	147.0	HFS
V I	6531.429	1.220	-0.840	131.6	137.6	72.9	143.3	...	105.5	...	135.2	174.3	162.4	HFS
V I	6531.429	1.220	-0.840	121.0	142.3	76.1	99.4	HFS
V I	6543.510	1.190	-1.660	66.0	80.6	94.5	92.3	...	49.9	...	59.2	142.6	100.8	HFS
V I	6543.510	1.190	-1.660	87.7	101.0	53.6	HFS
V I	6812.356	1.040	-2.110	69.5	91.3	36.0	51.0	39.5	56.8	126.1	...	HFS
Cr I	5296.700	0.980	-1.400	83.7	
Cr I	5296.700	0.980	-1.400	65.8	
Cr I	5348.340	1.000	-1.290	90.3	
Cr I	5787.930	3.320	-0.080	108.6	113.2	95.9	128.5	89.6	114.7	22.2	114.5	162.0	139.7	
Cr I	6330.096	0.940	-2.920	157.6	...	123.1	171.7	107.6	166.1	7.6	
Cr I	6881.716	3.440	-0.570	82.7	...	122.3	77.2	21.8	80.8	
Cr I	7400.188	2.900	-0.110	173.4	128.8	53.3	
Mn I	5516.670	2.180	-1.850	135.6	HFS
Mn I	6013.500	3.070	-0.250	SYN	SYN	SYN	SYN	SYN	SYN	SYN	SYN	HFS
Mn I	6016.640	3.070	-0.220	SYN	SYN	SYN	SYN	SYN	SYN	SYN	SYN	HFS
Mn I	6021.800	3.070	0.030	SYN	SYN	SYN	SYN	SYN	SYN	SYN	SYN	HFS
Co I	5301.030	1.710	-2.000	...	116.0	107.7	...	8.0	HFS
Co I	5483.350	1.710	-1.410	145.8	...	12.4	HFS
Co I	5483.350	1.710	-1.410	13.6	HFS
Co I	5530.710	1.710	-2.060	...	119.5	98.4	...	108.1	...	5.9	159.2	HFS
Co I	5647.230	2.280	-1.560	85.1	89.5	73.1	102.6	...	76.8	149.8	75.5	111.4	115.0	HFS
Co I	5647.230	2.280	-1.560	73.5	116.0	104.6	HFS
Co I	6188.998	1.710	-2.450	113.4	118.7	107.5	129.8	69.1	107.1	HFS
Co I	6188.998	1.710	-2.450	131.9	...	107.7	120.9	95.7	HFS
Co I	6678.849	1.960	-2.680	...	133.0	91.2	58.5	...	74.0	HFS
Co I	6678.849	1.960	-2.680	94.0	54.6	HFS
Co I	6770.970	1.880	-1.970	126.8	HFS
Co I	6814.961	1.960	-1.900	139.8	161.8	146.1	158.5	106.3	131.5	...	153.6	HFS
Co I	6814.961	1.960	-1.900	139.8	...	122.3	108.0	...	114.5	HFS
Co I	6872.440	2.010	-1.590	121.3	HFS
Co I	7417.390	2.040	-2.070	127.7	121.8	93.2	HFS
Ni I	4752.430	3.650	-0.700	94.1	186.7	...	
Ni I	5003.730	1.680	-2.800	109.3	125.3	66.8	...	9.9	
Ni I	5003.730	1.680	-2.800	101.9	13.9	
Ni I	5084.100	3.680	0.030	116.5	116.6	108.5	150.4	122.8	119.5	81.8	161.5	
Ni I	5084.100	3.680	0.030	99.7	94.6	120.0	113.8	77.5	155.4	
Ni I	5115.400	3.830	-0.110	...	61.9	142.3	97.8	173.9	135.0	
Ni I	5435.880	1.990	-2.590	109.6	111.3	125.0	...	25.1	...	186.7	174.1	
Ni I	5847.040	1.680	-3.210	117.5	129.8	...	138.3	98.1	114.7	7.0	120.2	174.6	174.5	
Ni I	6108.100	1.680	-2.450	171.3	169.4	123.8	...	168.9	...	35.9	
Ni I	6128.900	1.680	-3.330	114.9	110.9	109.0	140.4	81.7	
Ni I	6314.650	1.940	-1.770	148.2	136.7	114.0	166.1	142.3	177.3	36.2	
Ni I	6327.604	1.680	-3.150	131.1	134.0	124.4	163.7	122.6	151.7	11.4	150.5	
Ni I	6339.118	4.150	-0.550	83.7	21.7	88.6	
Ni I	6350.495	4.160	-1.810	19.3	19.0	20.5	25.2	...	26.2	...	37.4	
Ni I	6366.491	4.170	-0.950	...	161.4	136.8	73.2	12.3	76.4	
Ni I	6482.809	1.940	-2.630	130.9	144.5	122.4	...	115.4	139.8	8.0	
Ni I	6532.880	1.930	-3.390	84.7	93.5	78.3	85.3	7.0	86.1	170.6	157.4	
Ni I	6532.880	1.930	-3.390	84.9	101.2	94.5	85.5	
Ni I	6586.319	1.950	-2.810	122.6	121.8	119.6	138.4	100.6	133.7	14.1	...	187.0	...	
Ni I	6643.638	1.680	-2.300	52.6	
Ni I	6643.638	1.680	-2.300	51.0	
Ni I	6767.784	1.830	-2.170	159.8	174.9	157.2	...	51.7	

Table 3 — *Continued*

Species	λ (Å)	E.P. (eV)	log gf	EW	EW	EW	EW	EW	EW	EW	EW	EW	EW	Note
				(mÅ) 1978 737	(mÅ) 1978 730	(mÅ) 1866 954	(mÅ) 1866 1653	(mÅ) 1866 1667	(mÅ) 1711 831	(mÅ) 1711 988	(mÅ) 1711 1194	(mÅ) 2100 c12	(mÅ) 2100 b22	
Ni I	6772.321	3.660	-0.980	71.8	72.0	86.8	80.5	22.3	74.2	114.9	...	
Ni I	6914.500	1.950	-1.470	161.8	161.3	
Ni I	7062.900	1.950	-3.500	102.4	...	63.7	115.3	75.9	79.8	...	86.4	153.2	145.6	
Ni I	7110.905	1.940	-2.980	135.5	139.6	83.1	133.4	...	115.3	...	118.5	...	181.7	
Ni I	7122.206	3.540	0.040	158.8	164.5	...	146.5	81.3	
Ni I	7291.499	1.940	-2.780	179.7	184.2	
Ni I	7393.609	3.610	-0.270	128.5	129.0	77.8	150.9	71.0	154.4	107.0	88.5	
Ni I	7414.514	1.990	-2.570	161.8	165.0	168.3	187.4	29.1	
Ni I	7422.286	3.630	-0.140	136.5	129.6	137.1	63.7	
Ni I	7522.778	3.660	-0.400	142.6	143.1	131.6	51.0	
Ni I	7525.118	3.630	-0.520	104.6	113.3	115.8	105.4	41.0	180.1	
Ni I	7555.607	3.850	0.110	148.6	87.8	198.5	
Ni I	7555.607	3.850	0.110	122.2	
Cu I	5782.050	1.640	-2.920	SYN	SYN	SYN	SYN	SYN	SYN	HFS
Y I	6401.950	0.070	-2.180	17.6	28.6	...	22.4	...	9.0	...	9.7	...	21.2	
Y I	6435.049	0.070	-0.820	103.0	118.1	58.8	86.4	...	8.9	184.6	175.2	
Y II	4883.685	1.080	0.070	156.0	
Y II	5087.420	1.080	-0.170	116.7	119.0	101.6	114.1	120.0	133.6	77.5	155.4	
Y II	5087.420	1.080	-0.170	106.9	
Y II	5200.420	0.990	-0.570	116.5	13.9	
Y II	5509.910	0.990	-1.010	...	138.8	...	170.4	78.5	...	78.1	118.8	199.2	...	
Y II	6795.410	1.730	-1.250	29.2	83.0	19.1	37.3	41.7	39.4	37.9	36.0	89.5	...	
Y II	6795.410	1.730	-1.250	47.5	
Y II	7450.320	1.750	-0.780	25.5	42.0	26.9	...	88.4	75.0	
Ba II	5853.688	0.600	-1.010	SYN	SYN	SYN	...	SYN	SYN	SYN	SYN	HFS
La II	5114.510	0.240	-1.030	SYN	...	SYN	HFS
La II	6390.480	0.320	-1.520	SYN	SYN	SYN	SYN	SYN	SYN	SYN	SYN	SYN	SYN	HFS
Nd II	4959.190	0.060	-0.800	126.9	119.4	...	57.9	
Nd II	4959.190	0.060	-0.800	165.1	66.5	
Nd II	5092.800	0.380	-0.610	112.4	121.8	...	100.8	...	114.3	50.4	...	197.5	193.9	
Nd II	5092.800	0.380	-0.610	113.8	99.9	...	104.0	52.9	183.4	
Nd II	5212.350	0.200	-0.960	159.6	85.4	...	37.4	
Nd II	5249.590	0.980	0.220	85.2	109.5	...	187.7	94.3	
Nd II	5249.590	0.980	0.220	116.2	104.3	
Nd II	5255.520	0.200	-0.670	71.5	
Nd II	5255.520	0.200	-0.670	69.3	
Nd II	5293.180	0.820	0.100	120.5	147.0	95.6	...	83.7	
Nd II	5319.820	0.550	-0.190	147.3	142.5	...	165.3	120.2	...	82.7	...	187.3	...	
Sm II	4642.232	0.380	-0.520	SYN	
Eu II	6437.698	1.320	-0.270	SYN	SYN	SYN	...	SYN	SYN	SYN	SYN	SYN	...	HFS
Eu II	6645.127	1.380	0.200	SYN	SYN	SYN	SYN	SYN	SYN	SYN	SYN	SYN	SYN	HFS

Note. — Lines listed twice correspond to those measured in adjacent orders with overlapping wavelength coverage. Unless noted as “SYN”, all abundances are calculated with the listed EWs. Abundances that were calculated with hyperfine splitting of energy levels are noted as “HFS” in Column 15. References for line parameters are listed in Table 2.

Table 4
Comparison of Cluster IL to Stellar Results

Cluster	Neutral		Ionized	
	Offset	Scatter	Offset	Scatter
NGC 1978	-0.08	0.40	0.05	0.33
NGC 1866	-0.05	0.17	0.16	0.22
NGC 1711	0.17	0.18
NGC 2100	-0.07	0.29	0.03	0.26

Table 5
NGC 2019 Abundances

Species	$\log_{10}\epsilon(X)$	σ_{lines}	$[X/\text{Fe}]^1$	N_{lines}
O I	...	Lim	<1.00	1
Na I	5.00	0.17	0.50	3
Mg I	6.03	0.17	0.17	4
Al I	5.35	0.19	0.65	1
Si I	5.93	0.02	0.09	2
Ca I	4.85	0.05	0.21	16
Sc II	1.48	0.13	0.09	5
Ti I	3.38	0.09	0.15	12
Ti II	3.36	0.14	0.13	8
V I	2.35	0.24	0.02	3
Cr I	4.03	0.07	0.06	8
Mn I	3.61	0.11	-0.10	6
Fe I	5.83	0.03	-1.67	49
Fe II	5.85	0.04	-1.65	5
Co I	3.39	0.30	0.14	2
Ni I	4.50	0.07	-0.06	16
Sr II	-0.15	0.40	-1.40	1
Y II	-0.06	0.25	-0.60	1
Ba II	0.57	0.09	0.07	5
La II	-0.14	0.19	0.40	1
Nd II	0.48	0.21	0.70	2
Sm II	0.14	0.40	0.8	1
Eu II	-0.45	0.38	0.70	1

Note. — The error in the mean for N_{lines} is defined as $\sigma_{\text{lines}} = \sigma_X / \sqrt{N_{\text{lines}} - 1}$.

¹ For Fe this quantity is [Fe/H].

Table 6
NGC 2005 Abundances

Species	$\log_{10}\epsilon(X)$	σ_{lines}	$[X/\text{Fe}]^1$	N_{lines}
O I	...	Lim	<1.00	1
Na I	5.03	0.14	0.40	2
Mg I	5.99	0.20	-0.00	1
Ca I	5.04	0.08	0.27	6
Sc II	1.93	0.30	0.42	1
Ti I	4.08	0.47	0.72	2
Ti II	3.99	0.18	0.63	8
Cr I	4.19	0.18	0.09	3
Mn I	3.77	0.09	-0.08	2
Fe I	5.96	0.04	-1.54	34
Fe II	6.23	0.03	-1.27	4
Ni I	4.80	0.10	0.11	3
Ba II	1.10	0.30	0.47	1

Table 7
NGC 1916 Abundances

Species	$\log_{10}\epsilon(X)$	σ_{lines}	$[X/\text{Fe}]^1$	N_{lines}
O I	...	Lim	<1.00	1
Na I	5.33	0.28	0.70	2
Mg I	5.67	0.20	0.32	1
Al I	5.53	0.18	0.70	1
Si I	6.62	0.18	0.65	2
Ca I	5.15	0.10	0.38	7
Sc II	1.70	0.08	0.19	2
Ti I	3.91	0.16	0.55	2
Ti II	4.34	0.19	0.98	6
Cr I	4.20	0.12	0.10	5
Mn I	3.74	0.05	-0.10	6
Fe I	5.96	0.04	-1.54	50
Fe II	6.49	0.11	-1.01	3
Ni I	4.69	0.07	0.00	7
Sr II	0.84	0.40	-0.59	1
Y II	0.73	0.20	0.06	1
Ba II	0.78	0.30	0.15	2
Nd II	0.61	0.19	0.70	1
Eu II	0.21	0.20	0.70	1

Table 8
NGC 1718 Abundances

Species	$\log_{10}\epsilon(X)$	σ_{lines}	σ_{age}	σ_{Tot}	$[X/\text{Fe}]^1$	N_{lines}
Na I	5.52	0.16	0.15	0.22	0.05	3
Mg I	5.93	0.30	...	0.30	-0.90	2
Al I	5.82	0.20	...	0.30	0.15	1
Ca I	5.47	0.25	0.05	0.25	-0.14	3
Sc II	2.42	0.13	0.13	0.18	-0.39	1
Ti I	4.90	0.01	0.06	0.06	0.70	3
Cr I	5.19	0.30	...	0.30	0.25	1
Mn I	4.64	0.08	0.13	0.15	-0.05	2
Fe I	6.80	0.04	0.03	0.05	-0.70	69
Fe II	7.24	0.17	0.06	0.18	-0.26	4
Ni I	5.62	0.25	0.14	0.29	0.09	3
Y II	1.46	0.30	...	0.30	-0.05	1
Ba II	1.67	0.30	...	0.30	0.20	1

Table 9
NGC 1978 Abundances

Species	$\log_{10}\epsilon(X)$	σ_{lines}	σ_{age}	σ_{Tot}	$[X/\text{Fe}]^1$	N_{lines}
Na I	5.07	0.30	...	0.30	-0.57	3
Mg I	6.95	0.30	...	0.30	-0.05	1
Al I	...	Lim	Lim	Lim	<-0.15	1
Ca I	5.81	0.23	0.06	0.24	0.03	5
Ti I	4.17	0.27	0.09	0.29	-0.20	4
Ti II	4.98	0.22	0.21	0.31	0.16	2
V I	3.64	0.31	0.12	0.33	0.17	3
Mn I	4.72	0.14	0.06	0.15	-0.14	5
Fe I	6.96	0.06	0.18	0.19	-0.54	36
Fe II	7.55	0.09	0.11	0.14	0.05	4
Ni I	5.57	0.30	...	0.3	-0.10	1
Y II	2.08	0.30	...	0.30	0.40	1
Ba II	2.54	0.20	...	0.20	0.90	1
La II	1.25	0.16	...	0.16	0.65	1
Nd II	1.40	0.30	...	0.30	0.48	1

Table 10
NGC 1866 Abundances

Species	$\log_{10}\epsilon(X)$	σ_{lines}	σ_{age}	σ_{Tot}	$[X/\text{Fe}]^1$	N_{lines}
O I	8.83	0.30	...	0.30	0.20	2
Na I	5.58	0.20	...	0.20	0.23	3
Mg I	6.91	0.14	0.14	0.20	-0.27	3
Al I	6.93	0.25	...	0.25	-0.08	1
Si I	7.50	0.11	...	0.11	0.34	3
Ca I	6.14	0.06	0.14	0.15	0.18	7
Ti I	5.00	0.17	0.13	0.22	0.45	2
Ti II	5.01	0.10	0.19	0.21	0.31	2
V I	3.59	0.22	0.06	0.23	-0.06	2
Fe I	7.23	0.04	0.16	0.16	-0.27	50
Fe II	7.27	0.14	0.11	0.18	-0.23	8
Ni I	5.72	0.09	0.09	0.13	-0.16	7
Cu I	2.95	0.13	0.11	0.17	-0.91	2
Y II	1.95	0.20	...	0.20	0.10	1
Ba II	2.90	0.06	0.14	0.15	0.94	2
La II	1.56	0.04	0.06	0.07	0.71	2
Nd II	2.14	0.29	...	0.29	1.05	2
Sm II	1.18	0.30	...	0.30	0.70	1
Eu II	0.82	0.31	...	0.31	0.66	1

Table 11
NGC 1711 Abundances

Species	$\log_{10}\epsilon(X)$	σ_{lines}	σ_{age}	σ_{Tot}	$[X/\text{Fe}]^1$	N_{lines}
Ca I	5.71	0.30	0.30	0.43	-0.03	5
Mn I	4.71	0.12	0.12	0.17	-0.11	3
Fe I	6.93	0.08	0.07	0.11	-0.57	25
Fe II	6.62	0.18	0.05	0.19	-0.88	4
Ni I	5.90	0.05	0.07	0.09	0.24	5
Eu II	0.47	0.40	...	0.40	0.50	1

Table 12
NGC 2100 Abundances

Species	$\log_{10}\epsilon(X)$	σ_{lines}	σ_{age}	σ_{Tot}	$[X/\text{Fe}]^1$	N_{lines}
Al I	5.67	0.20	...	0.20	-0.55	2
Si I	7.56	0.30	...	0.30	0.20	2
Ca I	6.16	0.29	...	0.29	-0.19	10
Ti I	5.09	0.36	...	0.36	0.16	5
Ti II	4.42	0.36	-0.16	1
V I	4.22	0.42	...	0.41	0.19	9
Cr I	5.41	0.39	...	0.39	-0.26	4
Mn I	4.65	0.25	...	0.25	0.77	5
Fe I	7.53	0.08	...	0.08	0.03	30
Fe II	7.18	0.22	...	0.22	-0.32	5
Ni I	6.28	0.22	...	0.22	0.01	9
Y II	...	Lim	Lim	Lim	<-0.00	1
Ba II	2.08	0.30	...	0.30	0.22	1
Sm II	1.86	0.40	...	0.40	1.00	1
Eu II	0.77	0.30	...	0.30	0.40	1

Table 13
Abundance Ratios Measured in Individual Cluster Stars

Species		1978-737	1978-730	1866-954	1866-1653	1866-1667	1711-831	1711-1194	1711-988	2100-c12	2100-b22
O I	[O/Fe]	0.26	0.35	0.29	0.31	0.13	0.17	0.26	-0.09	...	0.03
	σ	0.10	0.20	0.10	0.10	0.10	0.10	0.20	0.10	...	0.20
	N _{Lines}	1	1	1	1	1	1	1	1	0	1
Na I	[Na/Fe]	0.11	-0.01	0.12	0.17	0.16	0.37	0.45	0.33	0.44	0.18
	σ	0.07	0.06	0.07	0.12	0.06	0.08	0.00	0.11	0.02	0.15
	N _{Lines}	3	4	2	5	4	4	2	4	2	2
Mg I	[Mg/Fe]	-0.04	0.03	-0.11	0.06	0.13	-0.00	0.17	-0.07	-0.13	-0.18
	σ	0.14	0.00	0.14	0.09	0.03	0.10	0.21	0.03	0.13	0.05
	N _{Lines}	3	3	2	3	3	3	3	3	2	3
Al I	[Al/Fe]	0.04	-0.04	-0.01	...	0.25	0.12	0.26	-0.14	0.06	-0.16
	σ	0.06	0.13	0.08	...	0.07	0.04	0.11	0.15	0.05	0.10
	N _{Lines}	4	3	2	0	2	3	2	1	2	3
Si I	[Si/Fe]	0.02	0.13	0.06	0.14	0.13	0.22	0.13	0.27	0.09	0.21
	σ	0.11	0.07	0.12	0.18	0.14	0.05	0.05	0.04	0.05	0.07
	N _{Lines}	7	9	8	2	3	16	9	11	7	7
Ca I	[Ca/Fe]	0.19	-0.00	0.07	-0.09	0.19	-0.00	0.00	0.34	0.22	-0.25
	σ	0.07	0.09	0.04	0.10	0.08	0.06	0.20	0.05	0.05	0.10
	N _{Lines}	8	9	9	5	11	9	3	14	3	4
Sc I	[Sc/Fe]	0.55	...	0.11	-0.33	0.57	0.22
	σ
	N _{Lines}	1	0	1	1	1	1	0	0	0	0
Sc II	[Sc/Fe]	0.14	0.11	0.27	0.33	0.24	0.25	0.22	0.41	0.14	-0.31
	σ	0.12	0.08	0.10	0.14	0.08	0.06	0.14	0.07	...	0.20
	N _{Lines}	5	7	5	5	6	7	3	4	1	1
Ti I	[Ti/Fe]	0.55	0.62	0.24	0.34	0.59	0.19	0.21	0.24	0.08	-0.02
	σ	0.07	0.10	0.09	0.07	0.07	0.06	0.14	0.04	0.17	0.07
	N _{Lines}	16	15	15	17	17	21	6	20	8	11
Ti II	[Ti/Fe]	0.22	0.65	0.35	0.25	0.37	-0.03	-0.06	0.03
	σ	...	0.38	0.12	0.13	0.04	0.05	0.05	0.04
	N _{Lines}	1	2	5	0	0	4	2	2	2	2
V I	[V/Fe]	0.06	0.06	-0.08	-0.04	0.47	-0.18	0.05	0.02	-0.14	-0.31
	σ	0.04	0.08	0.03	0.08	0.16	0.04	0.05	0.06	0.19	0.11
	N _{Lines}	9	9	17	8	7	6	4	5	3	3
Cr I	[Cr/Fe]	0.12	0.14	...	-0.11	0.19	-0.06	0.03	0.05	-0.10	-0.28
	σ	0.06	0.20	...	0.15	0.08	0.04	0.03	0.07	0.07	0.19
	N _{Lines}	4	1	0	2	2	4	2	7	2	2
Mn I	[Mn/Fe]	-0.32	-0.41	-0.38	-0.41	-0.28	-0.18	0.06	-0.35
	σ	0.06	0.05	0.04	0.07	0.05	0.06	0.11	0.05
	N _{Lines}	3	3	3	3	3	3	3	4	0	0
Co I	[Co/Fe]	-0.01	0.21	0.20	-0.10	0.48	-0.14	-0.04	-0.10	-0.35	-0.26
	σ	0.05	0.17	0.07	0.06	0.11	0.06	0.11	0.13	0.03	0.14
	N _{Lines}	5	7	8	4	7	9	4	4	2	3
Ni I	[Ni/Fe]	-0.01	0.12	-0.11	-0.25	-0.04	-0.10	0.07	-0.19	-0.10	-0.28
	σ	0.07	0.06	0.09	0.10	0.09	0.05	0.08	0.05	0.13	0.08
	N _{Lines}	25	22	13	10	15	26	11	27	7	12
Cu I	[Cu/Fe]	-0.64	-0.95	-0.81	-0.79	-1.00	-0.79
	σ	0.20	0.25	0.20	0.20	0.20	0.25
	N _{Lines}	1	1	1	1	1	0	0	1	0	0
Y I	[Y/Fe]	0.22	0.14	0.09	0.32	...	-0.07	0.04	...	0.13	-0.13
	σ	0.02	0.16	0.11	0.20	...	0.04	0.03	0.02
	N _{Lines}	2	2	2	1	0	3	2	0	1	3
Y II	[Y/Fe]	-0.09	0.75	-0.16	0.30	0.47	0.10	0.29	-0.14	0.25	0.40
	σ	0.17	0.20	0.19	0.15	0.20	0.12	0.05	0.18	0.19	0.15
	N _{Lines}	5	5	3	1	1	5	3	3	3	1
Ba II	[Ba/Fe]	0.77	0.88	0.90	...	0.52	1.04	1.09	0.86
	σ	0.25	0.20	0.08	...	0.30	0.25	0.25	0.20
	N _{Lines}	1	1	1	0	1	1	1	0	0	1

Table 13 — *Continued*

Species		1978-737	1978-730	1866-954	1866-1653	1866-1667	1711-831	1711-1194	1711-988	2100-c12	2100-b22
La II	[La/Fe]	0.42	0.31	0.54	0.64	0.40	0.67	0.62	0.41	0.60	0.29
	σ	0.20	0.20	0.10	0.15	0.18	0.15	0.15	0.10	0.20	0.20
	N _{Lines}	1	1	2	1	2	1	1	1	1	1
Nd II	[Nd/Fe]	1.04	1.15	...	0.87	0.86	0.51	...	0.36	0.64	0.44
	σ	0.18	0.18	...	0.28	0.12	0.12	...	0.06	...	0.09
	N _{Lines}	9	3	0	6	5	2	0	9	1	2
Sm II	[Sm/Fe]	1.08
	σ	0.07
	N _{Lines}	0	0	1	0	0	0	0	0	0	0
Eu II	[Eu/Fe]	0.29	0.16	0.33	0.64	0.17	0.40	0.52	0.19	0.45	0.29
	σ	0.18	0.10	0.14	0.20	0.18	0.18	0.14	0.18	0.21	0.10
	N _{Lines}	2	2	2	1	2	2	2	2	2	1

Note. — Uncertainties are defined as $\sigma = \sigma_X / \sqrt{N_{\text{lines}} - 1}$.

¹ For Fe this quantity is [Fe/H].

Table 14
Mean IL α Abundances for Milky Way Training Set and Old LMC GCs

	Milky Way	LMC (>10 Gyr)
[Ca/Fe]	+0.35 \pm 0.08	+0.29 \pm 0.09
[Ti/Fe]	+0.46 \pm 0.15	+0.55 \pm 0.37
[Si/Fe]	+0.52 \pm 0.20	+0.37 \pm 0.40
[$\alpha_{\text{CaTiSi}}/\text{Fe}$]	+0.44 \pm 0.09	+0.40 \pm 0.13